Georgia State University
ScholarWorks @ Georgia State University

Physics and Astronomy Theses | Department of Physics and Astronomy

4-22-2010

Measuring the Effective Wavelength of CHARA Classic

Emily Collins Bowsher
Georgia State University

Follow this and additional works at: http://scholarworks.gsu.edu/phy_astr_theses

Recommended Citation
Bowsher, Emily Collins, "Measuring the Effective Wavelength of CHARA Classic." Thesis, Georgia State University, 2010.
http://scholarworks.gsu.edu/phy_astr_theses/8

This Thesis is brought to you for free and open access by the Department of Physics and Astronomy at ScholarWorks @ Georgia State University. It has been accepted for inclusion in Physics and Astronomy Theses by an authorized administrator of ScholarWorks @ Georgia State University. For more information, please contact scholarworks@gsu.edu.

MEASURING THE EFFECTIVE WAVELENGTH OF CHARA CLASSIC

by

EMILY COLLINS BOWSHER

Under the Direction of Harold A. McAlister

Abstract

This thesis presents an engineering project measuring the effective wavelength of the CHARA Classic beam combiner on the CHARA Array. Knowing the actual effective wavelength of light observed is very important because that value is necessary for determining astrophysical parameters of stars. Currently, the value used for CHARA Classic data comes from a model of the system and is based on numbers published by the manufacturer of the filter; it is not derived from measurements done on the system directly. We use two data collection methods to observe standard stars of different spectral types and calculate the wavelength of light recorded by the instrument for each star. We find the best estimate of the effective wavelength for the CHARA Classic K'-band configuration to be $2.138 \pm 0.003 \mu m$, a 0.56% decrease from the previously adopted value of $2.150 \mu m$. Our result establishes the first estimate of the uncertainty in the effective wavelength.

INDEX WORDS: CHARA, Long baseline interferometry, Astronomical instrumentation, Effective wavelength, Stellar properties, Stellar diameters

MEASURING THE EFFECTIVE WAVELENGTH OF CHARA CLASSIC

by

EMILY COLLINS BOWSHER

A Thesis Submitted in Partial Fulfillment of Requirements for the Degree of

Master of Science

in the College of Arts and Sciences

Georgia State University

2010

Copyright by
Emily Collins Bowsher
2010

MEASURING THE EFFECTIVE WAVELENGTH OF CHARA CLASSIC

by

EMILY COLLINS BOWSHER

Committee Chair: Harold A. McAlister

Committee: Douglas R. Gies

Todd J. Henry

Russel J. White

Electronic Version Approved:

Office of Graduate Studies

College of Arts & Sciences

Georgia State University

May 2010

Dedication

This work is dedicated to my husband and everyone who believed in me and pushed me in this direction.

Acknowledgments

I would like to thank my family and friends for their love and support. I would like to thank my advisor for being so patient with me and accommodating as I completed much of this work after moving across the country. I would like to thank everyone I have worked with over the years for molding me into the scientist I have become.

I give many thanks to Tabetha Boyajian for graciously sharing her vast amount of 2008 CHARA Classic data with me without hesitation. I also want to thank Theo ten Brummelaar for suggesting this project to me and sharing his observing time with me when I was unable to collect data during my own nights. I want to thank PJ Goldfinger for trying so hard to get me data during my observing trip to the Array and Chris Farrington for actually collecting all of the data. Finally, I must thank my committee members for challenging me and providing such constructive feedback to improve this work.

Table Of Contents

Acknowledgments . . . . . **v**

List Of Tables . . . . . **viii**

List Of Figures . . . . . **ix**

List of Abbreviations . . . . . **x**

1 Introduction 1

1.1 Overview of CHARA Classic 1

1.2 Scientific Motivation 1

1.3 The Need for Empirical Measurement 5

1.4 Previous Calculations of the Effective Wavelength Value 6

1.5 This Project 8

2 Data Collection 10

2.1 Approach 10

2.2 Using the OPLE Carts for Fringe Scanning 10

2.3 Using the Dither Mirror for Fringe Scanning 12

3 Analysis 17

3.1 Approach 17

3.2 Data Collected Using OPLE Carts 17

3.3 Data Collected Using Dither Mirror 26

4 Results 28

4.1 Results from OPLE Cart Data 28

4.2 Results from Dither Mirror Data 35

4.3 Comparing OPLE Cart and Dither Mirror Results 40

4.4 Comparing Measured and Modeled Effective Wavelengths 42

5 Future Work 44

5.1 CHARA Classic Rebuild 44

5.2 Another Approach to Measuring the Effective Wavelength 45

6 Conclusion 47

References **48**

Appendices **49**

A Appendix A: OPLE Cart Data 50

B Appendix B: Dither Mirror Data 54

List Of Tables

1.1 Angular diameter dependence on effective wavelength 4

2.1 Data collected using the OPLE carts 12

2.2 Data collected using the dither mirror 14

4.1 Results calculated from the OPLE cart data. 30

4.2 Results calculated from the dither mirror data. 37

4.3 Overall Weighted Mean Results 41

4.4 Measured effective wavelength results compared with previous values. 42

A.1 Results from each data set of the OPLE cart data for HD 102647 51

A.2 Results from each data set of the OPLE cart data for HD 119850 51

A.3 Results from each data set of the OPLE cart data for HD 131156 52

B.1 Results from each data set of the dither mirror data 55

List Of Figures

1.1 CHARA Classic beam combiner layout. 2

1.2 The results of the model. 7

2.1 Altitude versus azimuth plot for each OPLE target 13

3.1 Position of the OPLE cart during a data set 19

3.2 OPLE cart position after the slope is removed. 20

3.3 Velocity of the OPLE cart during a data set. 20

3.4 Absolute value of the OPLE cart velocity. 21

3.5 An example scan showing the effects of fringe filtering. 24

4.1 Results for HD 102647 OPLE cart data taken 2009_05_19 31

4.2 Results for HD 102647 OPLE cart data taken 2009_06_01 31

4.3 Results for HD 119850 OPLE cart data taken 2009_06_01 32

4.4 Results for HD 131156 OPLE cart data taken 2009_05_19 32

4.5 Results for HD 131156 OPLE cart data taken 2009_06_01 33

4.6 Effective wavelength versus altitude plots for each OPLE target 35

4.7 Effective wavelength versus spectral type plot for all OPLE data 36

4.8 Effective wavelength versus altitude for all dither data 39

4.9 Weighted mean effective wavelength versus spectral type for dither data . . . 40

4.10 Effective wavelength versus baseline length for all dither data 41

4.11 Effective wavelength and bandwidth results for the two observing methods . 41

4.12 Comparing effective wavelength results with previous values. 43

List of Abbreviations

CHARA	Center for High Angular Resolution Astronomy
NPOI	Navy Prototype Optical Interferometer
OPLE	Optical Path Length Equalizer
QE	Quantum Efficiency

– 1 –

Introduction

1.1 Overview of CHARA Classic

Georgia State University's Center for High Angular Resolution Astronomy (CHARA) has a six-telescope optical/infrared interferometric array on Mt. Wilson in California. The six $1.0m$ telescopes are arranged in a Y-configuration, with two telescopes on each arm of the Y. The facility has been fully operational for science since 2005 and has the longest functioning infrared baseline in the world at $331m$. The entire CHARA Array system and facility is described in detail in ten Brummelaar et al. (2005).

The CHARA Array currently has six beam-combining instruments that combine the light from multiple telescopes. This work only addresses one of the beam combiners, CHARA Classic. CHARA Classic is a typical two-beam Michelson interferometer, which is the simplest and most classic type of beam combiner. It served as the first fringe optics for the Array and has historically been the most heavily used beam combiner. As shown schematically in the diagram of Classic (Figure 1.1), it combines the light from any two telescopes. CHARA Classic can observe in the H and K' band, but this project only concerns the effective wavelength when using the K' filter.

1.2 Scientific Motivation

The high angular resolutions achievable with interferometers make them well suited to measuring stellar diameters, distances, masses, and luminosities. In order to determine these astrophysical parameters of stars, astronomers calculate the calibrated visibility of the star from their observations. This visibility, arising from the uniform disk angular diameter of

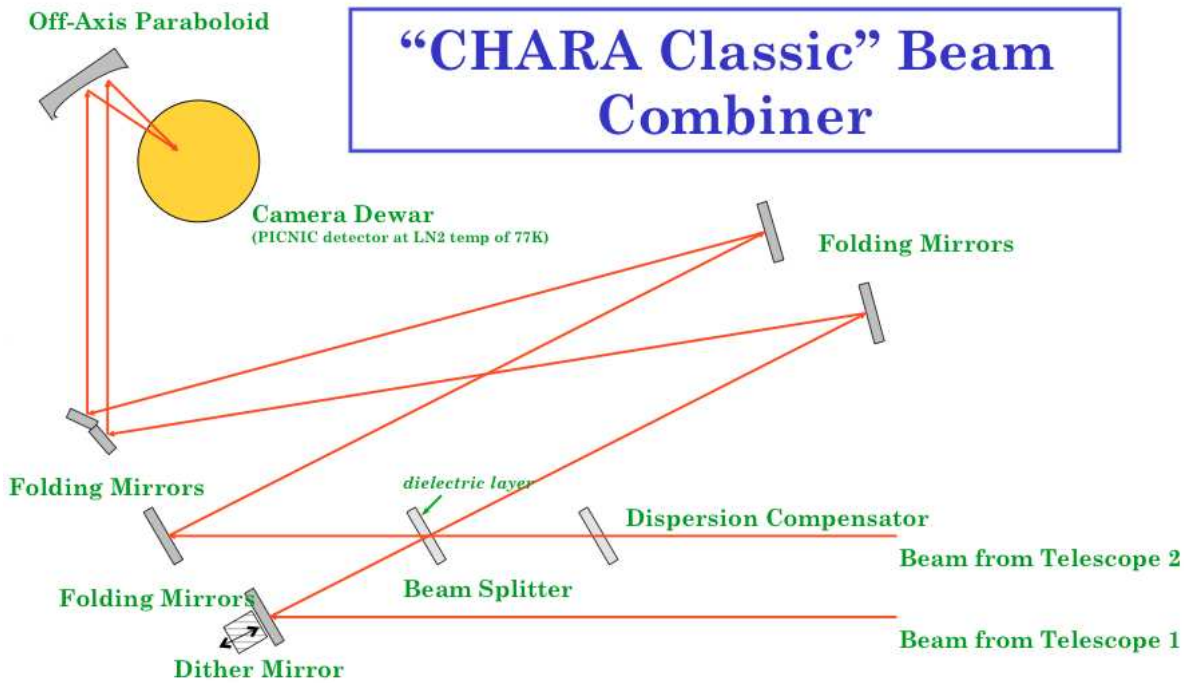

Figure 1.1: CHARA Classic beam combiner layout, showing the path of light through the system. (Figure courtesy of H. McAlister)

the star, is

$$V = 2\frac{J_1(\pi\Theta_{UD}B/\lambda)}{(\pi\Theta_{UD}B/\lambda)}, \tag{1.1}$$

where B is the baseline, λ is the effective wavelength, Θ_{UD} the angular diameter of the star (as modeled by a uniform disk), and J_1 is the 1st order Bessel function. From Equation 1.1, it is apparent that the visibility depends just as much on the effective wavelength λ as it does on the projected baseline value B. All data analysis methods require knowing these two parameters.

The lengths of the various baselines of the CHARA Array are known to better than $100nm$ accuracy and the zero path length condition is known to tens of nanometers at any given instance, making the uncertainty in the baseline astrometry negligible for the visibility calculation. A similar level of precision would be ideal for the effective wavelength

measurement. If the effective wavelength value is not accurate and precise, then it introduces systematic errors in the resulting stellar diameters and other astrophysical parameters measured with the Array.

Boyajian et al. (2008) and Baines et al. (2009) have both shown that the CHARA Array can measure angular diameters to better than 1%. However, those analyses do not take into account any uncertainty in the effective wavelength; it assumes the effective wavelength value used is known infinitely accurately.

Using the calibrated visibility and baseline values published in Boyajian et al. (2008) and Baines et al. (2009), we wanted to see what impact changes in effective wavelength have on the angular diameter results (see Table 1.1). The larger the calibrated visibility value (V_c), the less resolved the star. A calibrated visibility of 1.0 would mean the star is completely unresolved, while a value of 0.0 means the star is fully resolved. A 1% change in the effective wavelength can cause up to a 3σ change in the angular diameter for stars with smaller calibrated visibility values. The effects diminish as the calibrated visibility increases (and the star becomes less resolved); with larger calibrated visibility values, the angular diameter changes by less than 1σ with a 1% change in effective wavelength. Knowing the effective wavelength value to several tenths of a percent would allow angular diameter measurements to better than 1% for all calibrated visibility values.

Despite the fact that it has been the accepted practice of CHARA Classic users, assuming the effective wavelength value is infinitely accurate is dangerous because small changes in the effective wavelength value can cause large changes in the calculated angular diameter. Currently, the limiting factor in the accuracy of stellar angular diameter measurements is the effective wavelength value.

Table 1.1: Angular diameter dependence on effective wavelength

Star	mean V_c	$\lambda_{eff} = \lambda_{orig}$ Θ_{UD}	$\lambda_{eff} = \lambda_{orig} - 2\%$ Θ_{UD}	$\lvert\sigma_{ch}\rvert$	$\lambda_{eff} = \lambda_{orig} - 1\%$ Θ_{UD}	$\lvert\sigma_{ch}\rvert$	$\lambda_{eff} = \lambda_{orig} - 0.5\%$ Θ_{UD}	$\lvert\sigma_{ch}\rvert$	$\lambda_{eff} = \lambda_{orig} - 0.2\%$ Θ_{UD}	$\lvert\sigma_{ch}\rvert$
HD 222404[a]	0.09	1.923 ± 0.006	1.884 ± 0.008	6.50	1.903 ± 0.008	3.33	1.913 ± 0.006	1.67	1.919 ± 0.006	0.67
HD 188310[a]	0.11	1.671 ± 0.008	1.638 ± 0.007	4.13	1.654 ± 0.007	2.13	1.663 ± 0.008	1.00	1.668 ± 0.007	0.38
HD 221345[a]	0.26	1.297 ± 0.008	1.271 ± 0.008	3.25	1.284 ± 0.008	1.62	1.290 ± 0.008	0.87	1.295 ± 0.009	0.25
σ Dra[b]	0.46	1.224 ± 0.012	1.199 ± 0.011	2.08	1.211 ± 0.012	1.08	1.218 ± 0.012	0.50	1.222 ± 0.012	0.17
HD 199665[a]	0.53	1.073 ± 0.027	1.052 ± 0.027	0.78	1.062 ± 0.027	0.41	1.068 ± 0.027	0.19	1.071 ± 0.027	0.07
μ Cas A[b]	0.62	0.952 ± 0.009	0.932 ± 0.008	2.22	0.942 ± 0.009	1.11	0.947 ± 0.009	0.56	0.950 ± 0.009	0.22
HD 210702[a]	0.63	0.853 ± 0.017	0.836 ± 0.017	1.00	0.845 ± 0.017	0.47	0.849 ± 0.017	0.24	0.852 ± 0.017	0.06
HD 45410[a]	0.66	0.945 ± 0.033	0.927 ± 0.032	0.55	0.936 ± 0.033	0.27	0.941 ± 0.033	0.12	0.944 ± 0.033	0.03
HR 511[b]	0.76	0.747 ± 0.018	0.732 ± 0.018	0.83	0.740 ± 0.018	0.39	0.743 ± 0.018	0.22	0.746 ± 0.018	0.06
HD 217107[a]	0.78	0.688 ± 0.013	0.674 ± 0.013	1.08	0.681 ± 0.013	0.54	0.685 ± 0.013	0.23	0.687 ± 0.013	0.08
HD 154345[a]	0.84	0.491 ± 0.024	0.481 ± 0.024	0.42	0.486 ± 0.024	0.21	0.489 ± 0.024	0.08	0.490 ± 0.024	0.04
HD 185269[a]	0.88	0.471 ± 0.031	0.462 ± 0.031	0.29	0.467 ± 0.031	0.13	0.469 ± 0.031	0.06	0.470 ± 0.031	0.03
HD 16141[a]	0.90	0.480 ± 0.046	0.470 ± 0.045	0.22	0.475 ± 0.046	0.11	0.477 ± 0.046	0.07	0.479 ± 0.046	0.02

NOTES.—For stars of various calibrated visibilities V_c, the uniform disk angular diameter results are shown calculated with different effective wavelength values. The λ_{orig} effective wavelength value used for the first angular diameter calculation (column 3) is the current effective wavelength value for CHARA Classic (see Section 1.4). The remaining columns consider what impact the uncertainty level in λ_{orig} has on the angular diameter result. If the effective wavelength value is off by 2%, then by how many σ does the angular diameter change (column 4)? For each effective wavelength value (λ_{eff}), the calculated angular diameter (Θ_{UD}) is listed along with $|\sigma_{ch}|$, which represents the amount by which the Θ_{UD} changed (when compared to the initial Θ_{UD} result in column 3) in terms of the uncertainty in the initial Θ_{UD} result (column 3).

[a] Stars from Baines et al. (2009). [b] Stars from Boyajian et al. (2008).

1.3 The Need for Empirical Measurement

The wavelength of light measured by the instrument depends on more than just the filter used. Only about 5% of the light from a star actually arrives at the detector. Many factors have an effect on exactly which wavelengths of light make it to the detector and are collected by the instrument.

First, the target being observed, as with any object, emits more light at certain wavelengths than others. The Earth's atmosphere is not uniformly transmissive, meaning only certain wavelengths make it through (specifically optical, radio, and some parts of infrared; Carroll & Ostlie 1996). Once the starlight arrives at the Array, it encounters approximately two dozen optical surfaces (both reflective and transmissive) before the light gets to the beam combiner. These surfaces do not reflect or transmit 100% of the light at all wavelengths and the effect of the optical surfaces is not uniform for all wavelengths. Some wavelengths of light will be reflected by a mirror while other wavelengths will not be reflected and consequently will never arrive at the beam combiner. The mirrors along the light path are a combination of aluminum coated and silver coated mirrors. The wavelength dependence of light reflected by these mirrors changes as the coatings age.

Once the light arrives at the beam-combining instrument, it is further affected by the beam splitter, which reflects half of the light over to the dither mirror and transmits the other half of the light. As with the previous reflective and transmissive surfaces, only some wavelengths make it through this step. Only after the light enters the dewar does it travel through the actual filter intended to select only certain wavelengths of light. In our case this is a K' filter. Last, the quantum efficiency (QE) of the detector also plays a role. The

substances used in the detector are more sensitive to photons of some wavelengths than others.

Due to all of the effects mentioned above, one cannot predict the central wavelength by simply measuring the transmission of the filter itself. Data collected with the entire system working together as a whole (the Array with the instrument) are necessary to determine the wavelengths of light observed.

1.4 Previous Calculations of the Effective Wavelength Value

The value used for the effective wavelength prior to this project is a best-guess estimate derived from a model of the system developed by H. McAlister, D. Gies, and S. Ridgway. The model considers input wavelengths ranging from $1.850\mu m$ to $2.450\mu m$, in $0.025\mu m$ increments. For each wavelength, the model takes into account the wavelength dependence of the following factors: the estimated transmission of the Earth's atmosphere, transmission of the K' filter (as measured by the manufacturer), QE of the detector (as measured by the manufacturer), the transmission of the dichroic beam splitter (as measured by the manufacturer), the reflectivity of aged aluminum, and a relative flux (either of Regulus or a black body of a given temperature). These six factors are all multiplied together to give the effective transmission of the Array as a function of wavelength. Figure 1.2 shows how the six factors interact to determine the shape of the infrared filter.

The centroid of the effective transmission, or the effective wavelength of CHARA Classic with the K' filter, was calculated to be $2.150\mu m$. It was determined that the spectral type of the target observed had very little (0.03%) effect on the effective wavelength for stars with

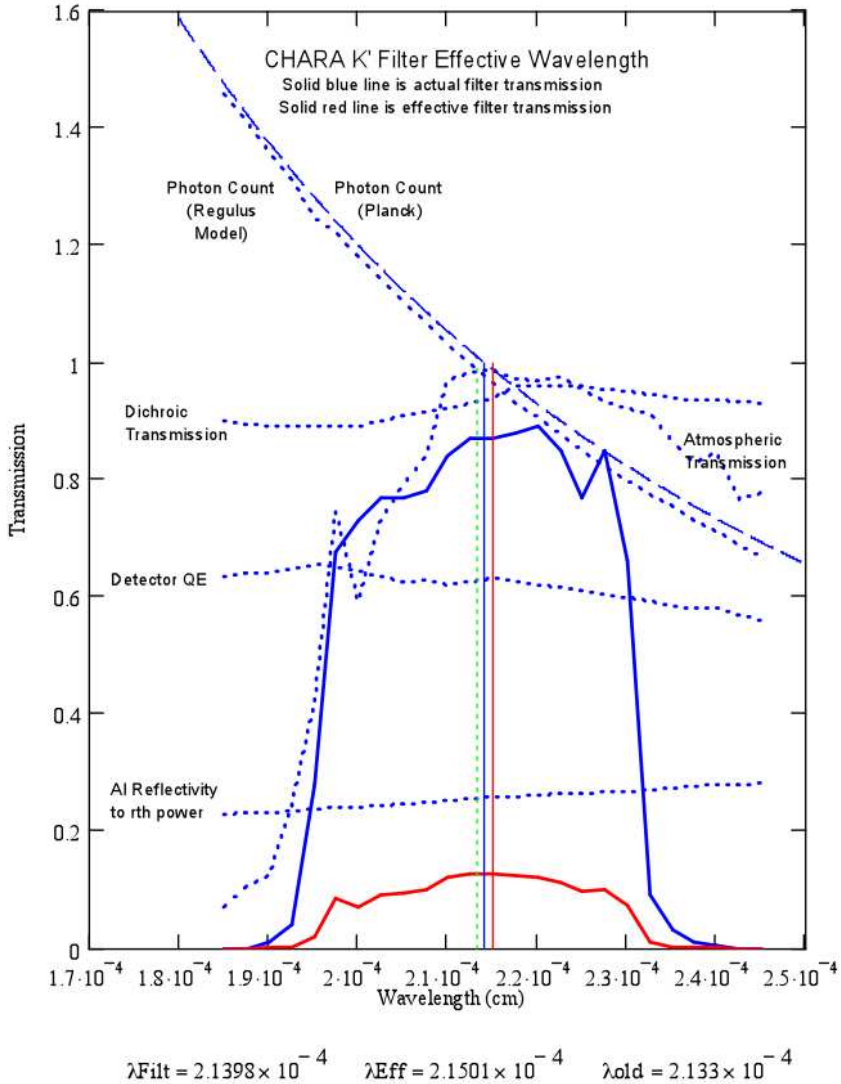

Figure 1.2: The results of the model showing the influence of various factors on the effective wavelength of the K' filter. The taller of the two solid line curves (blue solid line) is the wavelength dependence of the K' filter measured by the manufacturer. The flatter solid line curve (red solid line) is the effective transmission of CHARA Classic in the K'-band configuration as determined by the model. The centroid of this flatter curve (indicated by the vertical red solid line) is the $2.150\mu m$ effective wavelength value determined by the model. The three vertical lines (in order of increasing wavelength) are an older estimate of the effective wavelength (λold, green dotted line), the actual filter transmission (λFilt, blue solid line), and the modeled effective wavelength value (λEff, red solid line). (Figure courtesy of H. McAlister)

effective temperatures between 2,000 K and 10,000 K. Error estimation for this modeled effective wavelength value was never done.

There are some potential problems with this model. First of all, there are now some silver coated mirrors in the optical path in addition to the aluminum ones. The model would need to be modified to take into account the silver coated mirrors. A larger problem with the model is that the coatings on different mirrors age at different rates. All mirrors that are not in vacuum are recoated at the same time, but the coating on a mirror exposed to the elements (such as the primary) will age more quickly than the coating on a more sheltered mirror further down the optical path. It would be difficult to modify the model to use 'aged' reflectivity values for some mirrors and 'fresh' reflectivity values for other mirrors. Also, many of the wavelength dependence factors were 'as measured by the manufacturer,' meaning that those are the characteristics the manufacturer reports for the product. The specific item used in the CHARA Array could deviate some from the specifications.

The safest approach to knowing the effective wavelength of CHARA Classic is to actually measure it empirically. Depending on the results, measuring the effective wavelength could tell us more about the modeled value. We might have a better idea of how important certain factors, such as the ages of the mirror coatings, are in determining the effective wavelength.

1.5 This Project

The goal of this thesis is to measure empirically a more accurate and precise value for the effective wavelength of the CHARA Classic K' filter. The passband is the range of wavelengths that are transmitted through the Array and the instrument. The effective wavelength is the centroid of the passband, or the centroid of the effective transmission (see Figure 1.2). It is also useful to know what wavelengths of light on either side of the centroid arrive at the detector. In other words, it is useful to know the bandwidth or the

passband width of the Array. In addition to the effective wavelength, we will also measure the bandwidth value for the CHARA Classic K' filter. We determine the effective wavelength by measuring the separation between individual interference fringes in the fringe packet and we determine the bandwidth by analyzing the overall width of the fringe packet.

We employ two observational methods to measure these optical characteristics: using the Optical Path Length Equalizer (OPLE) carts to scan through the interference fringes and using the dither mirror in the beam combiner to scan through the interference fringes. The position of the OPLE cart is known to a greater precision than the position of the dither mirror (nm versus μm). Consequently, we believed the observations collected with the OPLE cart would yield a more precise effective wavelength measurement. However, as discussed later (Section 4), we find that the increased level of precision during data collection does not necessarily translate to increased precision in the measured effective wavelength.

– 2 –

Data Collection

2.1 Approach

The approach of this thesis is to observe stars of varying temperatures and calculate the effective wavelength for each star. Just as the peak wavelength of light emitted by a star increases for cooler stars, the effective wavelength value measured might also increase. In order to get the best signal to noise ratio, we want to observe bright, unresolved, non-multiple stars. We would also like to observe each of these stars at varying altitudes (horizon to zenith) in order to determine the effect, if any, of altitude on the wavelength of light observed. For example, water vapor in the atmosphere can increase the effective wavelength value. This effect would become more pronounced at larger airmasses because the star light travels through more atmosphere. If we detect an effective wavelength dependence on target temperature or altitude, then as CHARA users are reducing science observations, they can use the measured effective wavelength for a star of a similar temperature and altitude as their science target.

As previously mentioned, we employ two different methods for measuring the effective wavelength: using the OPLE carts to scan through the fringes and using the dither mirror to scan through the fringes. The data collection approach was different for the two observing methods.

2.2 Using the OPLE Carts for Fringe Scanning

The OPLE carts continuously move on their tracks during data collection, ensuring that the light from different telescopes travels an equal distance before it enters the beam combiner.

When using an OPLE cart to scan through the interferences fringes, the general behavior of the OPLE cart is no different than during regular Array operation. The difference between normal operation and using an OPLE cart to scan through the fringes is the motion of the dither mirror in the beam combiner. During normal operation, the dither mirror is constantly moving back and forth, scanning through the fringes. When an OPLE cart is used to scan the fringes, the dither mirror is completely stationary.

We decided to use the S1-S2 baseline because the combination of silver and aluminum coated mirrors is most similar to the setup that is planned for the rest of the Array (silver coatings for the mirrors in vacuum, aluminum coatings for the mirrors exposed to air). An added bonus in using S1-S2 is the short baseline ($34.08m$ on average), which means that most stars will be unresolved, giving us more target options.

We chose three bright, main sequence stars of varying spectral types: HD 102647 (A3V), HD 119850 (M2V), HD 131156 (G8V). These stars are all unresolved with S1-S2 and up for much of the evening during our observing period, allowing us to observe them at various altitudes. We did not observe any calibrator stars.

We were scheduled for two nights on the Array, 2009 May 5 and 6, but bad weather and technical issues prohibited observing. Theo ten Brummelaar and Chris Farrington graciously observed our targets during their scheduled nights in 2009 May and June. We obtained data for all three stars over two nights, 2009 May 19 and June 1, totaling 61 data sets. A data set is a file containing fringe packets from a given number of sequential scans. Table 2.1 details the observations taken using the OPLE carts to scan through the fringes. All three stars were observed 2009 June 1 while only two of the stars were observed 19 May 2009. During the first night of observations (2009_05_19), the S1 OPLE cart scanned the fringes while the

S2 cart served as the reference cart and remained stationary. Their roles reversed on the second night of observations (2009_06_01); the S2 cart scanned the fringes while the S1 cart remained stationary.

Table 2.1: Data collected using the OPLE carts to scan through the interference fringes.

HD	**SpType**	$\mathbf{m}_K$	**Date (UTC)**	**N**	**#scans**	**Alt Range (°)**
102647	A3V	1.88	2009_05_19	7	203	70.0 - 68.5
...	...	...	2009_06_01	18	503	66.5 - 56.8
119850	M2V	4.41	2009_06_01	15	384	70.2 - 63.6
131156	G8V	1.97	2009_05_19	7	161	67.7 - 70.6
...	...	...	2009_06_01	14	310	73.2 - 65.4

NOTES.—'N' is the number of data sets obtained that night while '# scans' is the number of individual scans (or fringe packets) in all data sets from that night. 'Alt range' shows the altitude (in degrees) of the star in the middle of the first data set and in the middle of the last data set of the night.

Due to the fact that we lost our observing time and our observations were worked into the schedule later, we did not collect data over the altitude range we were hoping. Our best altitude coverage is for HD 102647 (see Figure 2.1), but it only spans about 13° over the two nights. For HD 119850, the altitude coverage is less than 7° and it is just under 8° for HD 131156.

2.3 Using the Dither Mirror for Fringe Scanning

During normal operation of the beam-combining instrument CHARA Classic, a dither mirror scans through the interference signal repeatedly, searching for interference fringes. Rather than use valuable Array sky time collecting this normal type of Classic data, we chose to use data that had already been collected for other purposes. Not only does this save

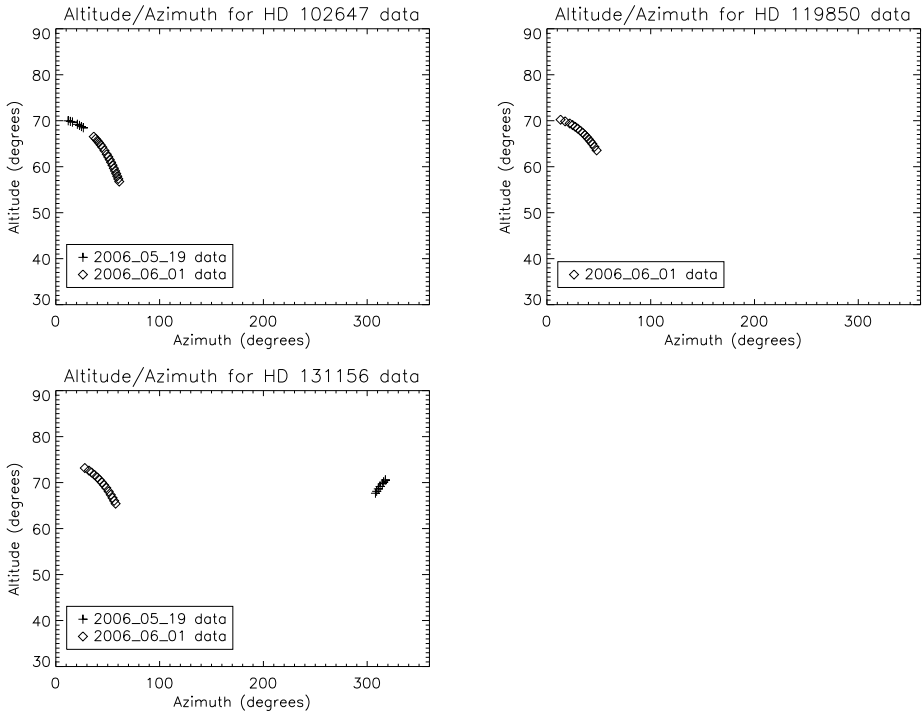

Figure 2.1: Altitude versus azimuth plot for each OPLE target. Top left: HD 102647, overall altitude coverage is 13.2°. Top right: HD 119850, overall altitude coverage is 6.6°. Bottom left: HD 131156, overall altitude coverage is 7.8°.

observing time, but it also provides us with more data than we would have been able to collect ourselves. Tabetha Boyajian graciously shared all of her 2008 CHARA Classic data with us. These data include 1501 total data sets for 107 different stars on 31 different nights and 6 different baselines, all collected with the K' filter. Again, a data set is a file containing fringe packets from a given number of sequential scans. We did not distinguish between which stars Boyajian used as calibrators and which stars were science targets; we considered all stars. Consequently, we have a mixture of resolved and unresolved targets. As previously stated, we would like our targets to be unresolved in order to get a higher signal to noise ratio. We do not believe that including some resolved stars in our sample of dither data will affect the effective wavelength measurement because such a large amount of data is going into the calculation. The amount of OPLE data is much smaller, making it important

that the targets observed using the OPLE carts are unresolved, giving higher signal to noise ratios.

We utilized a subset of Boyajian's 2008 Classic data for this project. We want the dither mirror observations to be as similar to the OPLE cart observations as possible. In an ideal situation, we would observe the same stars at varying altitudes using the same baseline. However, we do not have that luxury because we are using existing data. We selected which of Boyajian's data we would use based on spectral type. We included all observations for stars with spectral types similar to the spectral types of the stars we observed using the OPLE cart fringe scanning method. We utilized data from A2, A3, and A4 stars (to correspond with HD 102647), data from M0, M1, M2, and M3 stars (to correspond with HD 119850), and data from G6, G8, K0, and K1 stars (to correspond with HD 131156). These data encompass 224 data sets for 19 different stars on 17 different nights and 5 different baselines. Table 2.2 details the observations taken while using the dither mirror to scan through the fringes.

Table 2.2: Data collected using the dither mirror to scan through the interference fringes.

HD	**SpType**	**m_K**	**Date (UTC)**	**N**	**#scans**	**Alt Range (°)**	**Tel. used**
71	K0III	4.21	2008_10_24	7	1398	64.2 - 68.4	W1-E1
1326	M2V	4.02	2008_09_16	6	1382	75.0 - 65.1	E1-S2
			2008_09_17	12	2443	52.1 - 73.9	E1-S1
			2008_10_23	4	854	80.1 - 76.9	W1-E1
9407	G6V	4.89	2008_10_02	4	854	47.2 - 52.2	W1-E1
26965	K1V	2.50	2008_10_23	3	736	38.1 - 43.4	W1-E1
			2008_10_24	6	1195	32.5 - 43.7	W1-E1
36395	M1V	-	2008_10_23	2	596	44.1 - 50.3	W1-E1

Continued on next page

Table 2.2 – continued from previous page

HD	SpType	m_K	Date (UTC)	N	#scans	Alt Range (°)	Tel. used
79211	M0V	4.14	2008_10_22	5	1009	41.0 - 52.5	E1-S1
			2008_10_24	7	1405	44.5 - 64.2	W1-E1
102124	A4V	4.41	2008_04_19	10	3236	64.2 - 68.4	W1-S1
			2008_04_22	11	2404	54.6 - 63.9	E1-S1
114093	G8III	4.56	2008_04_21	13	4607	42.1 - 77.0	W1-S1
			2008_06_27	7	1405	63.5 - 51.3	E1-S1
131156	G8V	1.97	2008_04_18	5	1056	74.4 - 62.8	W1-S1
			2008_04_19	7	1859	57.2 - 72.3	W1-S1
			2008_06_27	9	1853	63.1 - 46.2	E1-S1
140775	A2V	5.43	2008_07_22	10	2343	60.3 - 48.1	E1-S1
141795	A2m	3.43	2008_07_22	8	1624	59.3 - 49.2	E1-S1
145607	A4V	5.05	2008_04_19	12	3332	41.3 - 40.2	W1-S1
			2008_04_21	6	2102	45.7 - 45.7	W1-S1
			2008_04_22	9	2024	36.6 - 47.2	E1-S1
			2008_04_23	7	1933	37.1 - 47.2	E1-S1
158633	K0V	4.51	2008_07_21	6	1342	40.8 - 35.5	E1-S1
167564	A4V	5.75	2008_04_22	7	1893	45.7 - 52.1	E1-S1
174897	K0	4.10	2008_07_22	6	1312	69.0 - 69.9	E1-S1
			2008_07_24	6	1320	70.2 - 65.9	E2-S1
182572	G8IV	3.04	2008_07_22	5	1024	64.2 - 67.3	E1-S1
			2008_07_24	5	1088	67.5 - 67.1	E2-S1
			2008_09_30	7	1385	66.2 - 51.6	E1-S1
204965	A3V	5.72	2008_10_02	3	703	68.4 - 70.8	W1-E1
214734	A3IV	4.91	2008_09_15	3	613	54.4 - 52.1	E1-S2
265866	M3	5.28	2008_10_22	4	1109	42.4 - 53.6	E1-S1
			2008_10_23	2	461	72.7 - 78.2	W1-E1

NOTES.—'N' is the number of data sets obtained that night while '# scans' is the number of individual scans (or fringe packets) in all data sets from that night. 'Alt range' shows the altitude (in degrees) of the star in the middle of the first data set and in the middle of the last data set of the night. 'Tel. used' indicates which telescope pair was used to collect the data.

Much of the time observations of the same star on different nights were collected with different telescope pairs, thus it does not make sense to assess the overall altitude coverage for targets over multiple nights. As previously mentioned, some telescopes have different mirror coating configurations in their optical path than others. With the available observations, it

would be impossible to determine whether a change in effective wavelength was due to the change in telescopes or due to the altitude change of the target.

– 3 –

Analysis

3.1 Approach

This was one of the first CHARA Classic projects to use the OPLE carts to scan through interference fringes instead of the dither mirror. During all CHARA Classic observing, the dither mirror position (in μm) is written to file every millisecond. When the dither mirror is turned off (as it is when using the OPLE carts to scan for fringes), the dither mirror position of $0.00\mu m$ is written to file every millisecond. All of the data reduction software developed for CHARA Classic requires relevant dither mirror position information and chokes when a user inputs data without appropriate dither mirror positions. We modified our data analysis process to work around this issue.

The meat of our data analysis is based on the process discussed in Benson et al. (1995) and ten Brummelaar et al. (2005). The foundation of the analysis, described below, is the same for the two types of data, but the execution details differ.

3.2 Data Collected Using OPLE Carts

As previously mentioned, the data taken when using the OPLE carts to scan through the interference fringes is missing the position information that is normally recorded by the dither mirror. Normally, the dither mirror position information enables us to determine the position and velocity of the interference fringes and consequently the fringe frequency. Without this information, we cannot extract any results from our data. We needed to find a work-around to compensate for the missing information before we could analyze the data.

One of the data analysis software tools used for CHARA Classic is a Mathcad program written by H. McAlister called VisUVCalc. By developing alternative means of determining the fringe position and velocity, we modified this program so it accepts data without dither mirror positions.

Owing to the fact that the dither mirror positions are normally used to determine the location of each fringe, our first task was to figure out how to locate the fringes without that information. Using the modified VisUVCalc program, we visually examine each data set in its entirety and record the position of each fringe (based on a visual estimate) in a text file. We then read the fringe position file into the Mathcad program and the data set is broken into individual scans, one for each fringe. The scan is centered at the recorded fringe position and includes 512 data points before that position and 512 points after it. The system records a data point once every millisecond. Therefore, each scan is 1025 milliseconds long. The visually determined fringe positions are accurate to within 200 milliseconds.

We needed another work-around to determine how often the fringes were sampled, or the velocity of the fringes. Luckily, every half a second during observations the system records the position (in m) of each OPLE cart along the track in a log file. If we use this information to calculate how fast the cart is moving, then we will have an idea of the velocity of the fringes. However, a bit of data manipulation is required before the fringe velocity can be determined from the information recorded.

As shown in Figure 3.1, the motion of the cart follows a sloped saw-tooth pattern. The slope is due to the OPLE cart compensating for the change in optical path length between the two telescopes caused by the telescopes tracking the star as the Earth rotates. In other words, the slope is the result of the OPLE cart doing its normal job and has nothing to do

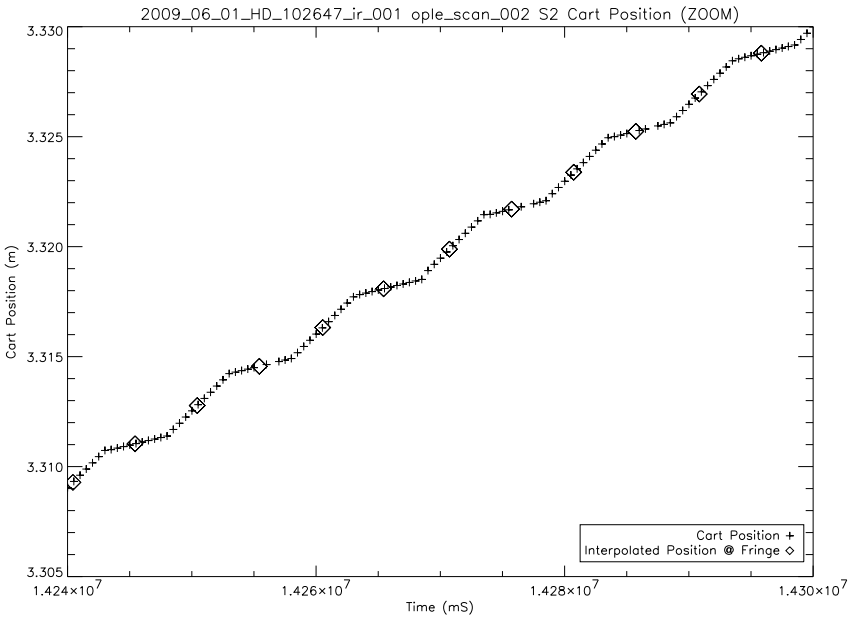

Figure 3.1: The position of the OPLE cart during a data set has a sloped saw-tooth pattern. This plot is zoomed in on a portion of the data set in order to clearly display the saw-tooth pattern. The diamond points indicate the location of the OPLE cart when a fringe was recorded.

with scanning for fringes. Using IDL's `poly_fit` function, we do a 1st degree least-squares polynomial fit to capture the general sloping trend. We then subtract the sloping trend from the position data. The result, as seen in Figure 3.2, is a much flatter saw-tooth pattern. One can clearly see the back and forth motion of the OPLE cart as it scans through the interference fringes. The fringes are recorded roughly in the middle of the cart's back and forth motion.

To calculate the velocity of the OPLE cart, we use IDL's `deriv` function to perform numerical differentiation on the flattened position values and their corresponding times from the OPLE log file. Figure 3.3 shows the resulting velocity. The vast majority of the velocity data points are located in the horizontal portions of the plot where the fringes are recorded

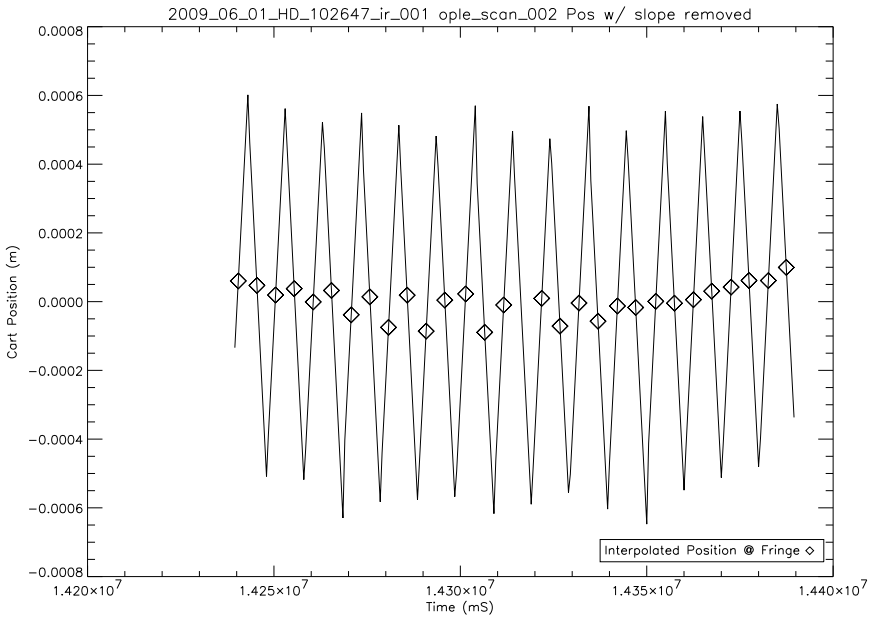

Figure 3.2: OPLE cart position after the slope (see Figure 3.1) is removed. The diamond points indicate the location of the OPLE cart when a fringe was recorded.

(indicated by diamonds on the plot). The cart spends most of the time moving at a fairly constant speed and quickly changes direction to scan through the fringe again.

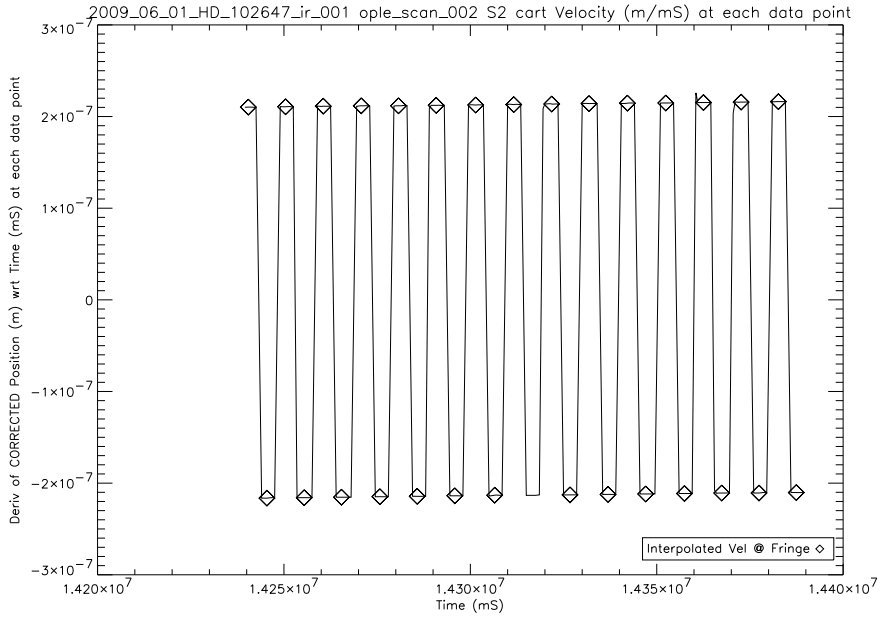

Figure 3.3: Velocity of the OPLE cart during a data set. The diamond points indicate when a fringe was recorded.

We believe that the fringes should always occur when the cart's velocity is fairly constant, during the flat parts on velocity plots. As previously mentioned, the fringe times should be accurate to 200 milliseconds. Things should work perfectly because we have velocity data for the OPLE cart every 500 milliseconds. However, sometimes the fringes seem to occur while the cart changes direction, during the vertical parts in Figure 3.3. It is not clear whether this is actually the case, or whether the appearance of this is the result of an inconsistency in the system. It is possible that atmospheric turbulence is shifting the fringe and causing it to appear in this position.

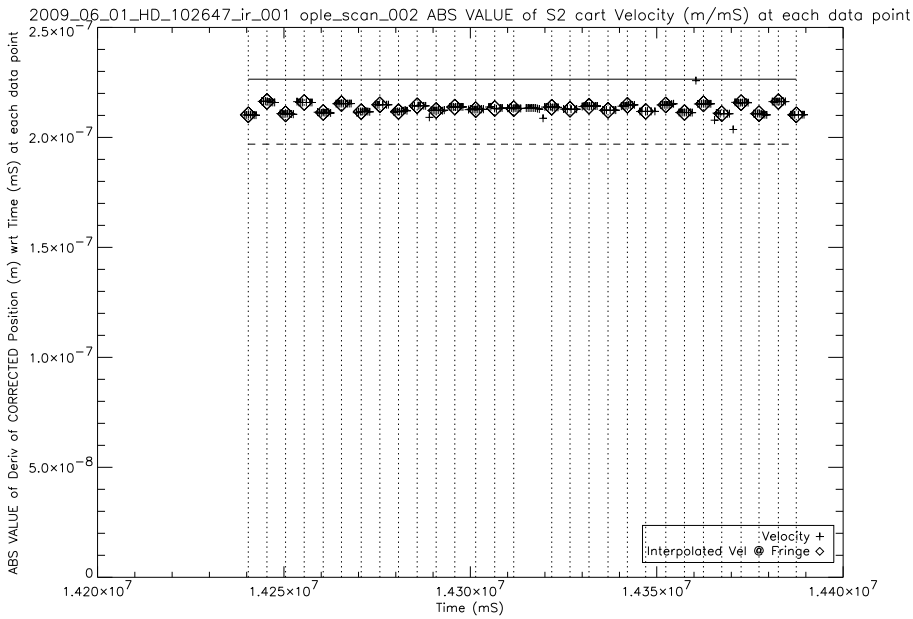

Figure 3.4: The absolute value of the OPLE cart velocity (plotted as individual points +) appears as a nearly flat line with a slight X pattern. All points above the solid horizontal line and below the dashed horizontal line were discarded. The diamond points and the vertical dotted lines indicate the time at which a fringe was recorded. The velocity values of the diamond points are saved to a file and used as the velocities of the fringes.

For the fringe velocity, we are really only interested in the speed of the OPLE cart and not whether the cart was moving toward or away from the detector when the fringe was recorded. Therefore, the absolute value of the cart velocity is the value we are after. In order

to determine the velocity of the cart when the fringe was recorded, we use IDL's `interpol` function to interpolate the velocity at the time of the fringe based on the absolute value velocity data for the times in the OPLE cart position log file. One can see in Figure 3.4 that the absolute value of the velocity is plotted as individual data points (+) as opposed to a line as in Figure 3.3. The data points along the vertical lines in Figure 3.3 end up as scatter in the absolute value plot. These scatter points throw off the interpolation for the cart velocity at the time of the fringe because, as previously mentioned, the fringe occasionally appears during this velocity transition time when the cart changes direction. To help mitigate this situation, we throw out the data points that appear as scatter in the absolute value of the velocity. As shown in Figure 3.4, we discard all data points above the solid horizontal line and all points below the dashed horizontal line. Everything above the solid horizontal line is greater than 15% above the average absolute value velocity for the entire sample (including the scatter). The dashed horizontal line is placed at the average absolute value velocity. After removing these scatter points, the velocity points interpolated for the fringe times fall where they should, during the times when the cart velocity is constant.

For each data set, we save these interpolated velocity values to a text file. We further modified the VisUVCalc program to read in the fringe velocities from the text file and use that information in place of the dither mirror positions for the rest of the data analysis. After being so careful to determine the velocity of the OPLE cart at exactly the time when the fringe was recorded, we planned to use the individual velocities for each fringe in the rest of the data reduction. However, we found that using the mean of the fringe velocities as the velocity for each fringe packet generally yields more precise results. This means that it is better to eliminate the slight X pattern seen in the absolute value of the velocities

(Figure 3.4). More work is required to determine exactly why the slight X pattern appears and why it does not seem to be indicative of the actual velocity of the cart.

Once we have the fringe position text file and the fringe velocity text file, we can proceed with more standard CHARA Classic data analysis techniques. The VisUVCalc program breaks the raw data into individual scans, one for each fringe packet, as previously mentioned. We apply a low pass filter to each scan by doing a Fourier transform on the data, resulting in a smoothed version of the scan. The low-pass filtering removes all of the high frequency phenomena in the data (including the fringes) and keeps only the low frequencies, which are due to effects such as atmospheric seeing and piston error. In order to remove these low frequency characteristics from the data, we normalize each raw scan with the low pass filtered version of itself.

We further smooth the signal by passing each normalized scan through a bandpass filter. The bandpass filter serves to clean up the oscillations of the fringe by removing noise in the vicinity of the fringe scanning frequency. It removes some detector noise and high frequency noise from sources such as instrumental vibrations. Figure 3.5 follows a sample fringe through the steps of the filtering process.

In order to extract any information from the data, we must find an equation to fit the fringe packets. Using Mathcad's built-in `genfit` function, each fringe is fitted to the fringe expression

$$V \frac{\sin(\pi \Delta\sigma t)}{\pi \Delta\sigma t} \cos(2\pi\sigma_0 t + \phi), \tag{3.1}$$

where V is the visibility, $\Delta\sigma$ is the coherence length $(\Delta\lambda/\lambda^2)$, determined by the width of the spectral bandpass, σ_0 is the wavenumber $(1/\lambda_0)$, determined by the center of the spectral

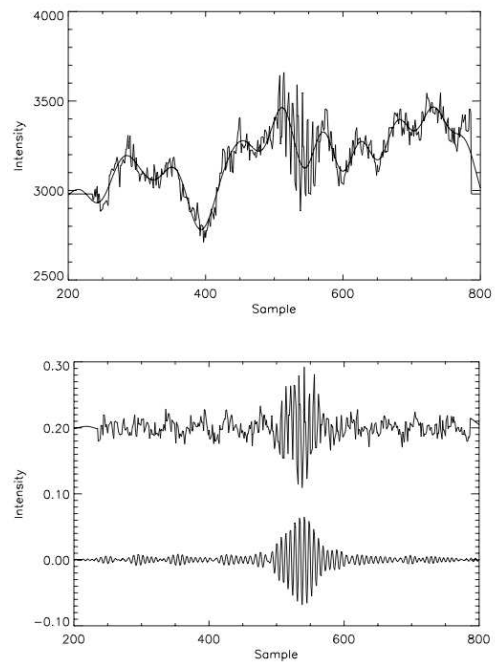

Figure 3.5: An example scan showing the effects of fringe filtering. Top: The jagged line is the raw data with the low-pass filtered version of itself (smooth line) superimposed. Bottom: The same scan after normalization (top) and after bandpass filtering (bottom). The two are offset by 0.2 for increased readability. (Figure from ten Brummelaar et al. 2005)

bandpass, ϕ is an atmospheric induced phase shift, and t is time. It should be noted that the version of the fringe equation in both Benson et al. (1995) and ten Brummelaar et al. (2005) contains another parameter v_g for the group velocity of the fringe packet. That parameter is not needed in our fringe equation because we have fixed the fringe velocity to the mean of the velocity values determined from the OPLE cart position information. We instead incorporate our fringe velocity values into the time parameter in the equation. Meaning, the time parameter we pass into `genfit` is actually $t \cdot v_g$, where v_g is the mean of our fringe velocities.

The Mathcad program fits the equation to each fringe packet five separate times. It uses the highest amplitude peak as the center of the fringe packet for the first fit. However, the highest amplitude peak is not necessarily the center of the fringe packet, thus the fit is

recalculated four times using neighboring peaks as the center of the packet. The neighboring peaks used in the recalculations are the two peaks to the left of the highest amplitude peak and the two peaks to the right of the highest amplitude peak. Out of the five fits, the one with the highest ratio of visibility to root mean square of residuals of the fit is considered the 'best' fit and that fringe fit is selected. The results of the fringe fit include best fit values for the coherence length ($\Delta\sigma$), wave number (σ_0), and atmospheric induced phase shift (ϕ) variables in Equation 3.1.

We manually examine each individual fringe packet and its best fit, assessing the quality of the fringe and the fit. We reject malformed, asymmetric, and very weak fringes. The fringes that are discarded are not used in any further calculation.

We use the results of the best fringe fit to calculate the optical characteristics of CHARA Classic in which we are interested: the effective wavelength and the bandwidth. We utilize the wave number term to calculate the wavelength of light observed for each fringe packet with the equation

$$\lambda_0 = 1/\sigma_0. \tag{3.2}$$

This value is averaged for all 'good' fringes, resulting in the mean effective wavelength λ_{eff} for the whole data set. Because `genfit` does not provide errors for the fitted parameters, the average of the standard deviation of each λ_0 value from the mean is used for the mean effective wavelength error $\sigma\lambda_{eff}$. The λ_{eff} value represents the centroid of the effective transmission of CHARA Classic.

Another parameter calculated while fitting the fringe is the coherence length. As done with the observed wavelength of light, the program calculates the mean coherence length for all 'good' fringes and calculates the error from the average standard deviation.

The mean effective wavelength value and the mean coherence length value are both used to calculate the average bandwidth, or how many microns of light on both sides of the effective wavelength make it through the instrument. From the equation for coherence length,

$$\Delta\sigma = \frac{\Delta\lambda}{\lambda^2}, \tag{3.3}$$

it follows that the bandwidth ($\Delta\lambda$) can be calculated from the mean effective wavelength (λ_{eff}) and the mean coherence length ($\Delta\sigma$):

$$\Delta\lambda = \Delta\sigma \cdot \lambda_{eff}^2. \tag{3.4}$$

In summary, the fringe fitting process determines the best fit values for the wave number and coherence length parameters. The mean effective wavelength is then calculated from the wave number. Once the mean effective wavelength is known, the bandwidth, or passband width, is determined from the coherence length.

3.3 Data Collected Using Dither Mirror

The analysis for the data collected using the dither mirror to scan through the fringes is much more akin to the standard CHARA Classic data reduction process as described by ten Brummelaar et al. (2005).

The dither mirror position values provide enough information for VisUVCalc to locate the fringe packets and break each data set up into scans, one for each fringe packet. Each

scan goes through a low-pass filter and the raw scan is then normalized against the low-pass version of itself (Figure 3.5). The normalized scan is then bandpass filtered. Each fringe packet is fit to the fringe expression

$$V\frac{\sin(\pi\Delta\sigma v_g t)}{\pi\Delta\sigma v_g t}\cos(2\pi v_g\sigma_0 t+\phi), \tag{3.5}$$

where v_g is the group velocity of the fringe packet and V, $\Delta\sigma$, σ_0, ϕ, and t are as defined in Equation 3.1. We do not fix the velocity value as we did in Equation 3.1 because this group velocity is due to the motion of the dither mirror and we have access to the dither mirror position information. From the dither mirror information, we can determine an initial guess for the v_g value to pass into `gen_fit` for the fringe fitting. The VisUVCalc program determines the final velocity value from the results of the fringe fit.

The VisUVCalc program locates the highest amplitude peak in each fringe packet and takes that peak to be the center of the fringe packet. The program then performs the fringe fitting around that highest amplitude peak.

The effective wavelength and bandwidth are calculated the same way as in Section 3.2, when the OPLE cart was used to scan through the fringes.

– 4 –

Results

We wanted to measure empirically the effective wavelength of CHARA Classic to several tenths of a percent (ideally to 0.2%). If the effective wavelength is known to this level, then the uncertainty in the effective wavelength value enables angular diameter measurements to better than 1%.

We expected the data taken while using the OPLE cart to scan through the fringes to yield a more precise result because the OPLE cart position is known to greater precision than the position of the dither mirror ($10^{-9}m$ versus $10^{-6}m$). However, the final results from the two methods have comparable precision.

4.1 Results from OPLE Cart Data

We calculate the mean effective wavelength (λ_{eff}) and bandwidth ($\Delta\lambda$) values for each data set individually as discussed in Section 3.2. Using the individual data set results we then calculate weighted mean results for each star on each night. In the weighted mean, the amount each data point contributes to the average is determined by the error associated with that data point. We use the square root of the variance of the weighted mean as the estimated error for the weighted mean. We calculate the weighted mean for data sets $i = 1 \ldots N$ using

$$\overline{\lambda_{eff}} = \frac{\sum_i^N (\frac{\lambda_{eff_i}}{\sigma\lambda_{eff_i}^2})}{\sum_i^N (\frac{1}{\sigma\lambda_{eff_i}^2})}, \tag{4.1}$$

$$\overline{\sigma\lambda_{eff}} = \sqrt{\frac{1}{\sum_i^N (\frac{1}{\sigma\lambda_{eff_i}^2})}}, \tag{4.2}$$

and the analogous bandwidth equations.

Figures 4.1, 4.2, 4.3, 4.4, and 4.5 show the mean effective wavelength and bandwidth values calculated for each data set as well as the weighted mean values for each star each night. The error for the weighted means are significantly smaller than the error values for the individual data sets.

Table 4.1 gives the weighted mean results from the data using the OPLE cart to scan through the fringes. See Appendix A for detailed tables containing the results from the individual data sets. The seventh column in Table 4.1 gives a measure of the level of accuracy of the mean effective wavelength calculation by listing the error $\overline{\sigma\lambda_{eff}}$ as a percentage of the calculated $\overline{\lambda_{eff}}$ value. This is the value we would like to see around 0.2%, but it is larger for all of our results.

Reduced χ^2 analysis (column 8 in Table 4.1) shows our error estimations for the mean effective wavelength are too conservative in most cases. A reduced χ^2 value of 1.0 would mean that the error estimations were appropriate, a value less than 1 indicates the errors are over estimated, while a reduced χ^2 value greater than 1 means the errors are under estimated. We calculate the reduced χ^2 value from the individual data sets for each star each night and not from the weighted mean value. The estimated error in the weighted mean values for each star each night are significantly smaller than the errors in the individual data sets (see Figures 4.1 - 4.5), indicating that our reduced χ^2 values will be much less than one. The fact that we did not achieve the level of precision we had hoped might be due in part to our error estimation methods.

Table 4.1: Results calculated from the OPLE cart data.

HD	**Spec Type**	$\mathbf{m}_K$	**Obs Date (UT)**	**N**	**#scans used**	$\overline{\lambda_{eff}}$ (μm)	$\overline{\sigma\lambda_{eff}}$ (%)	χ^2_ν	$\overline{\Delta\lambda}$ (μm)
102647	A3V	1.88	2009_05_19	7	105	2.137 ± 0.019	0.89	0.19	0.338 ± 0.010
...	...	...	2009_06_01	18	257	2.126 ± 0.006	0.28	0.13	0.332 ± 0.003
119850	M2V	4.41	2009_06_01	15	97	2.138 ± 0.006	0.28	0.46	0.335 ± 0.004
131156	G8V	1.97	2009_05_19	7	74	2.144 ± 0.013	0.61	0.72	0.335 ± 0.009
...	...	...	2009_06_01	14	125	2.154 ± 0.005	0.23	2.74	0.335 ± 0.003

NOTES.— The mean effective wavelength ($\overline{\lambda_{eff}}$) and bandwidth ($\overline{\Delta\lambda}$) values for each star are the weighted mean of the results from the individual data sets. 'N' is the number of data sets obtained that night. The '#scans used' column indicates the number of individual scans (or fringe packets) that were utilized for the effective wavelength and bandwidth calculations. The reduced χ^2 (χ^2_ν) value is calculated from the individual data sets from that star on that night. See Appendix A for the results from the individual data sets.

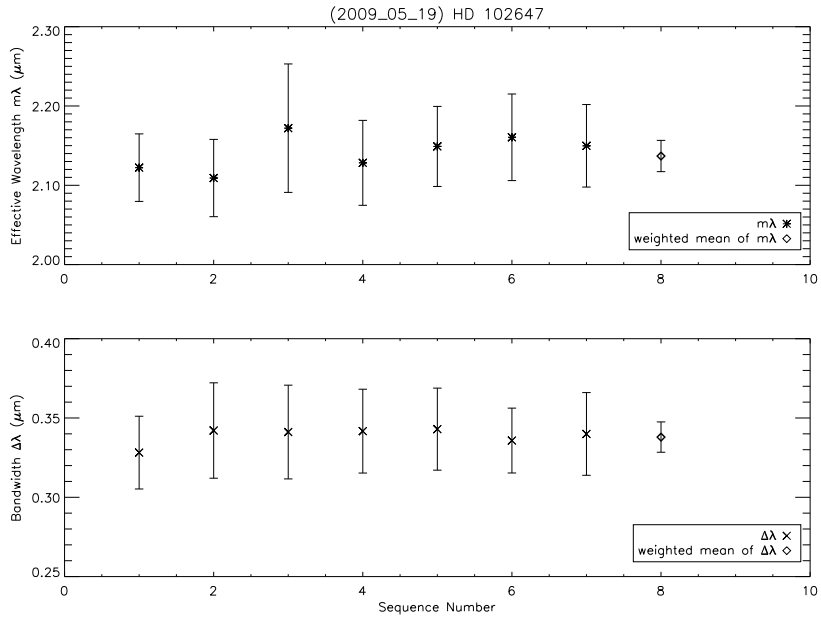

Figure 4.1: Results for HD 102647 OPLE cart data taken 2009_05_19. Top: Mean effective wavelength for each data set and the weighted mean value of those data sets (shown at the end of the sequence). Bottom: The width of the passband for each data set and the weighted mean value of those data sets.

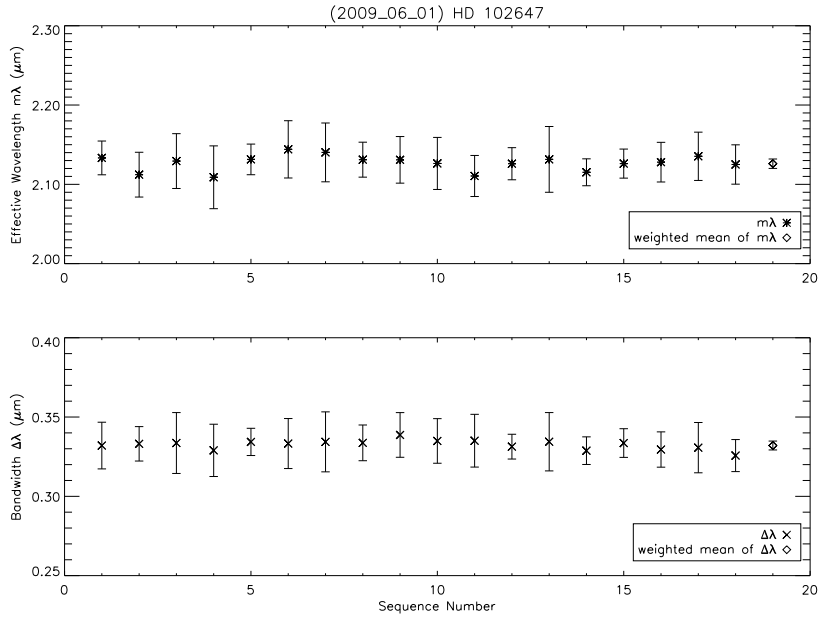

Figure 4.2: Results for HD 102647 OPLE cart data taken 2009_06_01. Top: Mean effective wavelength for each data set and the weighted mean value of those data sets (shown at the end of the sequence). Bottom: The width of the passband for each data set and the weighted mean value of those data sets.

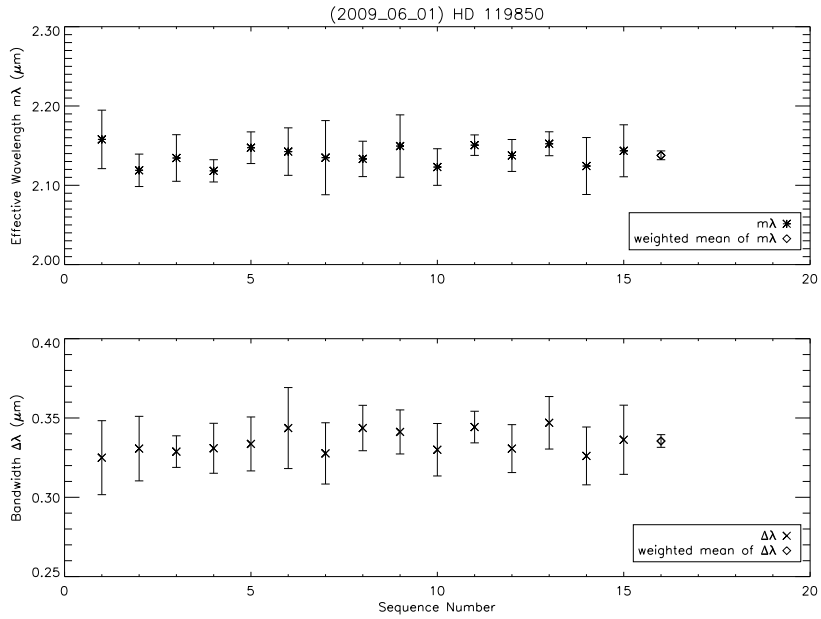

Figure 4.3: Results for HD 119850 OPLE cart data taken 2009_06_01. Top: Mean effective wavelength for each data set and the weighted mean value of those data sets (shown at the end of the sequence). Bottom: The width of the passband for each data set and the weighted mean value of those data sets.

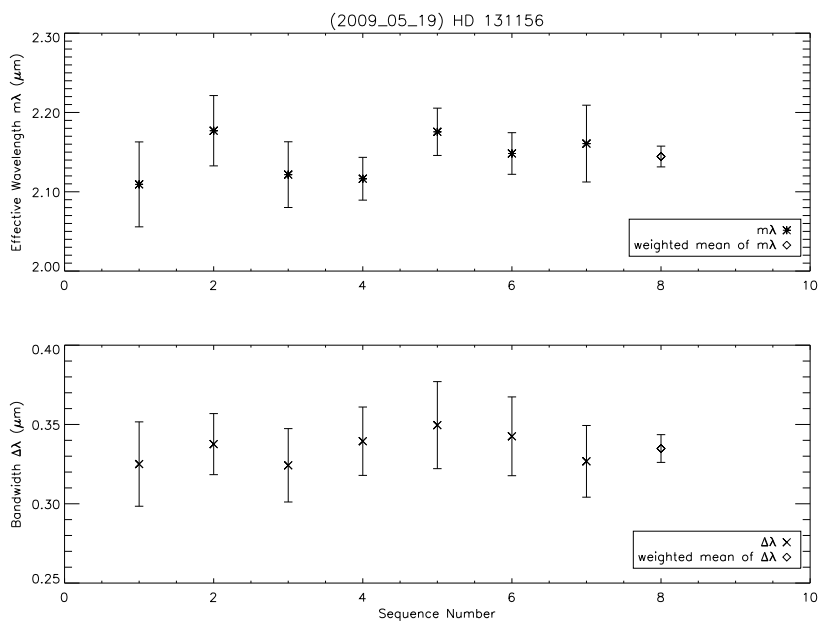

Figure 4.4: Results for HD 131156 OPLE cart data taken 2009_05_19. Top: Mean effective wavelength for each data set and the weighted mean value of those data sets (shown at the end of the sequence). Bottom: The width of the passband for each data set and the weighted mean value of those data sets.

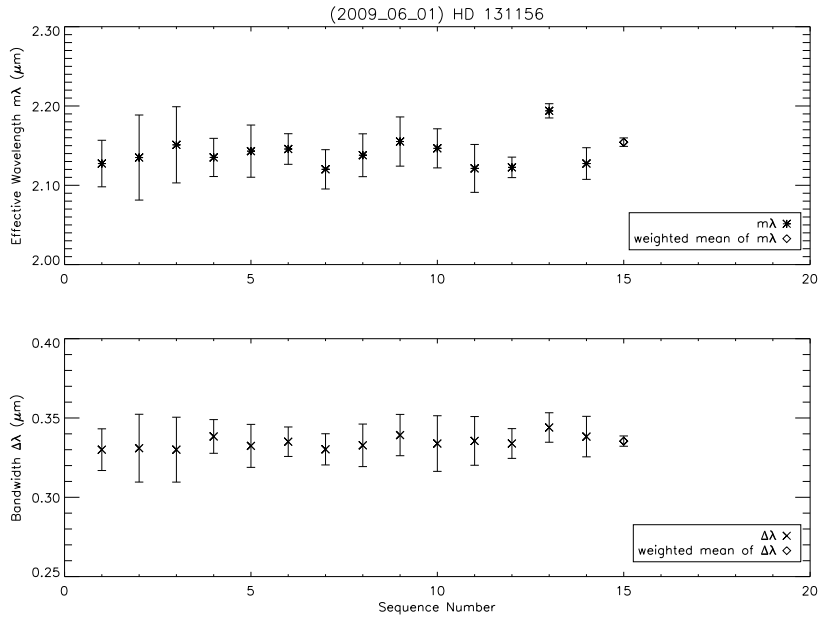

Figure 4.5: Results for HD 131156 OPLE cart data taken 2009_06_01. Top: Mean effective wavelength for each data set and the weighted mean value of those data sets (shown at the end of the sequence). Bottom: The width of the passband for each data set and the weighted mean value of those data sets.

It should be noted that two subsets of data had anomalous OPLE cart velocity calculations. To account for this, we fixed the fringe group velocity value for these data as opposed to using the mean of the fringe velocities determined from the OPLE log file (see Section 3.2). The fringe velocity values calculated from the OPLE cart position information are inaccurate for the HD 119850 and HD 131156 data taken 2009_06_01. For these data, the mean fringe velocity is around 1.6x$10^{-7} m/millisec$ instead of around 2.13x$10^{-7} m/millisec$ as with the rest of the data. We have no explanation for the slower velocity values. The VisUVCalc program is unable to find adequate fits for any of the fringes when using this slower velocity value. However, when we use a faster velocity value calculated for different data, the Mathcad program finds suitable fits for all of the fringes. Therefore, for the

HD 119850 and HD 131156 data taken 2009_06_01, we fixed the fringe group velocity to 2.133x$10^{-7} m/millisec$, the average of the mean fringe velocity values of the other data sets.

The conditions during the second night of observations (2009_06_01) allowed for more precise results than the conditions on the first night (2009_05_19). Despite that, the lack of precision in our results coupled with not having as many observations as we originally planned hampered our ability to achieve our goals. We do not detect a noticeable change in the effective wavelength due to target elevation angle or spectral type.

Figure 4.6 contains plots of the effective wavelength over the altitude ranges observed for each star. There is no discernible trend in the effective wavelength, but the altitude coverage is extremely limited. Figure 4.7 shows the results in terms of effective wavelength and spectral type. The results are grouped by spectral type in decreasing temperature order. No trend between object spectral type and effective wavelength is clear.

Going into the project, we thought there was a good chance that target temperature and elevation would not have a large impact, if any, on the effective wavelength value. The large error bars on our results prevent us from ruling for sure that there is no impact on the effective wavelength value. The effective wavelength could change with target temperature and elevation, but we were unable to detect it at our level of precision and altitude coverage.

We decided to calculate the weighted mean of all data sets collected using the OPLE cart to scan the fringes. If the effective wavelength does not depend on spectral type or elevation angle, then there is no reason to only report results separated by that criteria. The overall weighted mean value for the effective wavelength and bandwidth are given in Table 4.3. When all 61 OPLE cart data sets are averaged together, the uncertainty in the effective wavelength value decreases to 0.14%. Using this effective wavelength value would

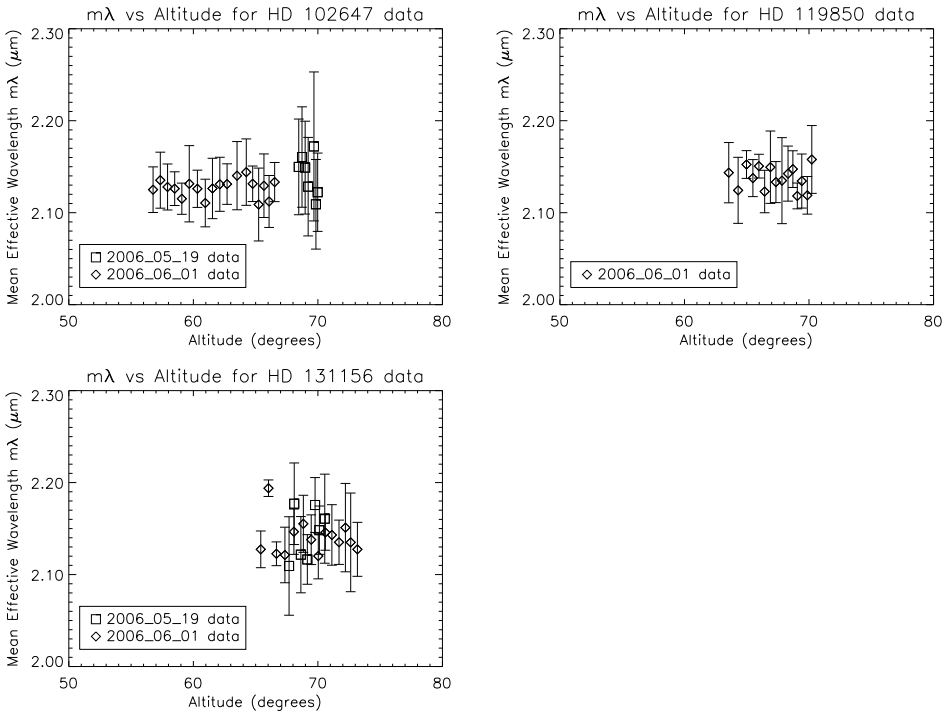

Figure 4.6: Effective wavelength versus altitude plots for each OPLE target. Data from both nights are plotted. No change in effective wavelength is detected over the altitude range observed. Clockwise from top left: HD 102647, HD 119850, HD 131156.

enable CHARA Classic users to accurately measure stellar angular diameters to better than 1%. Also, reduced χ^2 analysis for all of the OPLE cart data sets together gives a result of nearly 1.0, indicating that, when all of the data are considered as a whole group, our error analysis results are appropriate.

4.2 Results from Dither Mirror Data

The results from the data collected using the dither mirror to scan through the interference fringes are similar to the results found from the OPLE cart data. There are considerably more observations for the dither mirror data, both in number of data sets and in number of scans (individual fringe packets). However, it is much more difficult to analyze the results

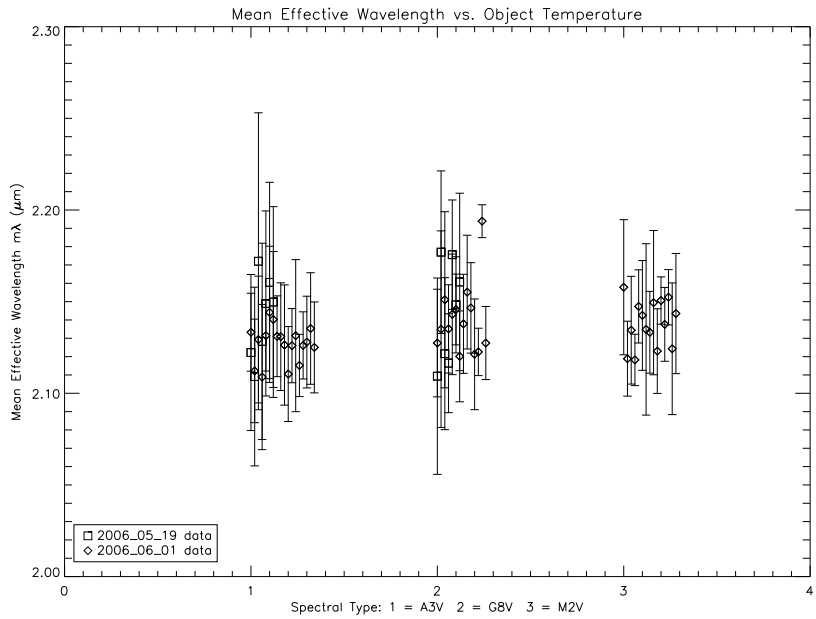

Figure 4.7: Effective wavelength versus spectral type plot for all OPLE data. No change in effective wavelength is detected with a change in object temperature. The objects are plotted by decreasing temperature based on their spectral type. All of the results for HD 102647 are clustered around 1.0 on the plot because it is an A3V star. HD 131156 results are clustered around 2.0 (G8V) and HD 119850 around 3.0 (M2V). The spacing between the observations of the same star is simply for increased readability.

of these data because they are so varied (19 different stars, 17 different nights, 5 different telescope pairs).

Table 4.2 gives the weighted mean values for the effective wavelength and bandwidth for each star each night. We calculate the weighted mean values and their errors as shown in Equations 4.1 and 4.2. The uncertainty in the effective wavelength measurement is on average more than 50% larger for the dither results than the OPLE results, but the reduced χ^2 values are almost all smaller. The reduced χ^2 analysis indicates that the error estimates for the effective wavelengths are much too large and over estimated more than the error estimates for the OPLE cart results.

Table 4.2: Results calculated from the dither mirror data.

HD	**Spec Type**	$\mathbf{m}_K$	**Obs Date (UT)**	**N**	**#scans used**	$\overline{\lambda_{eff}}$ (μm)	$\overline{\sigma\lambda_{eff}}$ (%)	χ^2_ν	$\overline{\Delta\lambda}$ (μm)	**Tel. used**
71	K0III	4.21	2008_10_24	7	769	2.132 ± 0.009	0.42	0.14	0.340 ± 0.009	W1-E1
1326	M2V	4.02	2008_09_16	6	723	2.146 ± 0.019	0.89	0.10	0.387 ± 0.030	E1-S2
			2008_09_17	12	1401	2.141 ± 0.011	0.51	0.12	0.346 ± 0.011	E1-S1
			2008_10_23	4	447	2.138 ± 0.018	0.84	0.07	0.355 ± 0.024	W1-E1
9407	G6V	4.89	2008_10_02	4	484	2.129 ± 0.020	0.94	0.13	0.352 ± 0.017	W1-E1
26965	K1V	2.50	2008_10_23	3	357	2.143 ± 0.029	1.35	0.06	0.370 ± 0.047	W1-E1
			2008_10_24	6	716	2.140 ± 0.013	0.61	0.11	0.328 ± 0.009	W1-E1
36395	M1V	-	2008_10_23	2	281	2.131 ± 0.031	1.45	-[a]	0.375 ± 0.054	W1-E1
79211	M0V	4.14	2008_10_22	5	644	2.131 ± 0.014	0.66	0.19	0.340 ± 0.014	E1-S1
			2008_10_24	7	809	2.142 ± 0.013	0.61	0.11	0.345 ± 0.009	W1-E1
102124	A4V	4.41	2008_04_19	10	1462	2.154 ± 0.016	0.74	0.03	0.438 ± 0.032	W1-S1
			2008_04_22	11	1303	2.128 ± 0.011	0.52	0.15	0.357 ± 0.009	E1-S1
114093	G8III	4.56	2008_04_21	13	1932	2.145 ± 0.015	0.70	0.02	0.449 ± 0.037	W1-S1
			2008_06_27	7	782	2.127 ± 0.010	0.47	0.10	0.344 ± 0.012	E1-S1
131156	G8V	1.97	2008_04_18	5	579	2.147 ± 0.020	0.93	0.08	0.369 ± 0.023	W1-S1
			2008_04_19	7	942	2.147 ± 0.020	0.93	0.05	0.412 ± 0.035	W1-S1
			2008_06_27	9	1022	2.136 ± 0.009	0.42	0.17	0.344 ± 0.008	E1-S1
140775	A2V	5.43	2008_07_22	10	1273	2.141 ± 0.012	0.56	0.13	0.359 ± 0.015	E1-S1
141795	A2m	3.43	2008_07_22	8	887	2.139 ± 0.013	0.61	0.18	0.356 ± 0.011	E1-S1
145607	A4V	5.05	2008_04_19	12	1694	2.144 ± 0.016	0.75	0.03	0.411 ± 0.025	W1-S1
			2008_04_21	6	816	2.152 ± 0.023	1.07	0.01	0.444 ± 0.043	W1-S1
			2008_04_22	9	1101	2.140 ± 0.013	0.61	0.12	0.360 ± 0.014	E1-S1
			2008_04_23	7	942	2.142 ± 0.019	0.89	0.05	0.412 ± 0.035	E1-S1
158633	K0V	4.51	2008_07_21	6	728	2.142 ± 0.016	0.75	0.07	0.351 ± 0.019	E1-S1
167564	A4V	5.75	2008_04_22	7	1022	2.138 ± 0.015	0.70	0.03	0.368 ± 0.030	E1-S1

Continued on next page

Table 4.2 – continued from previous page

HD	Spec Type	m_K	Obs Date (UT)	N	#scans used	$\overline{\lambda_{eff}}$ (μm)	$\overline{\sigma\lambda_{eff}}$ (%)	χ^2_ν	$\overline{\Delta\lambda}$ (μm)	Tel. used
174897	K0	4.10	2008_07_22	6	670	2.129 ± 0.015	0.70	0.11	0.359 ± 0.017	E1-S1
			2008_07_24	6	707	2.127 ± 0.012	0.56	0.22	0.347 ± 0.015	E2-S1
182572	G8IV	3.04	2008_07_22	5	541	2.132 ± 0.014	0.66	0.29	0.356 ± 0.018	E1-S1
			2008_07_24	5	565	2.126 ± 0.014	0.66	0.23	0.347 ± 0.018	E2-S1
			2008_09_30	7	797	2.127 ± 0.013	0.61	0.09	0.345 ± 0.011	E1-S1
204965	A3V	5.72	2008_10_02	3	374	2.126 ± 0.022	1.03	0.12	0.347 ± 0.039	W1-E1
214734	A3IV	4.91	2008_09_15	3	321	2.122 ± 0.023	1.08	0.02	0.356 ± 0.022	E1-S2
265866	M3	5.28	2008_10_22	4	567	2.124 ± 0.019	0.89	0.01	0.359 ± 0.030	E1-S1
			2008_10_23	2	239	2.129 ± 0.027	1.27	-[a]	0.364 ± 0.035	W1-E1

NOTES.— The mean effective wavelength ($\overline{\lambda_{eff}}$) and bandwidth ($\overline{\Delta\lambda}$) values for each star are the weighted mean of the results from the individual data sets. 'N' is the number of data sets obtained that night. The '#scans used' column indicates the number of individual scans (or fringe packets) that were utilized for the effective wavelength and bandwidth calculations. The reduced χ^2 (χ^2_ν) value is calculated from the individual data sets from that star on that night. 'Tel. used' indicates which telescope pair was used to collect the data. See Appendix B for the results from the individual data sets.

[a] χ^2_ν cannot be calculated for N≤2

Again, we do not detect a change in the effective wavelength due to target altitude (Figure 4.8) or target spectral type (Figure 4.9). There is also no discernible difference in the effective wavelength value measured from different baselines or telescope pairs (Figure 4.10).

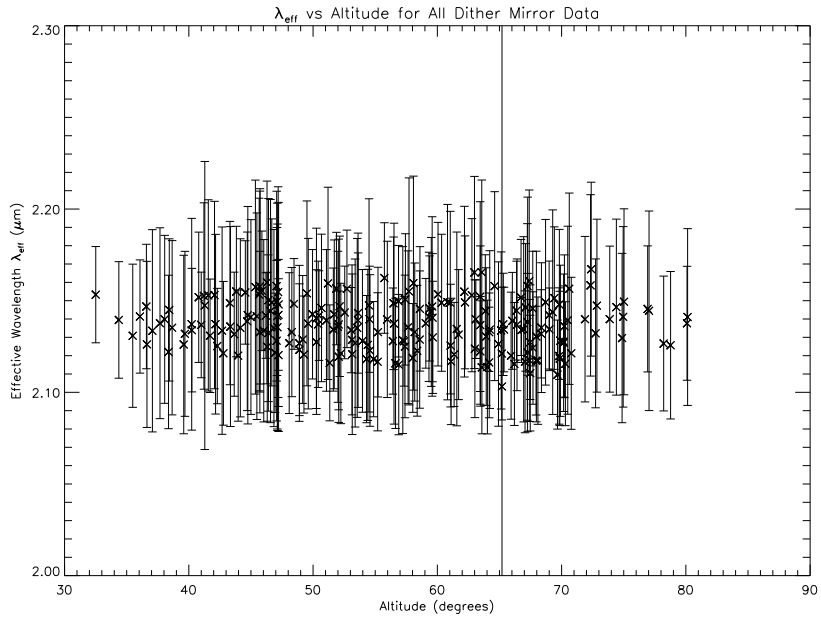

Figure 4.8: Effective wavelength versus altitude for all observations collected using the dither mirror. No change in effective wavelength is detected. The error bar that goes off the plot has a value of $0.553\mu m$ and belongs to data set 8 of the HD 114093 observations from 2008_04_21.

As with the OPLE cart data, the lack of precision in our results prevents us from stating for certain that the effective wavelength value is not dependent on the target spectral type, target altitude, or the baseline and telescopes with which the target is observed. Even if these effective wavelength dependences exist, we thought it would be very difficult to detect them with our dither mirror data because the data themselves are so varied. Neither the spectral type, the altitude, nor the telescopes used were kept constant at any time, thus we do not have a clean basis of comparison.

We calculated the weighted mean of all of the data sets collected with the dither mirror (see Table 4.3). The uncertainty in the effective wavelength decreases to a pleasing 0.09%,

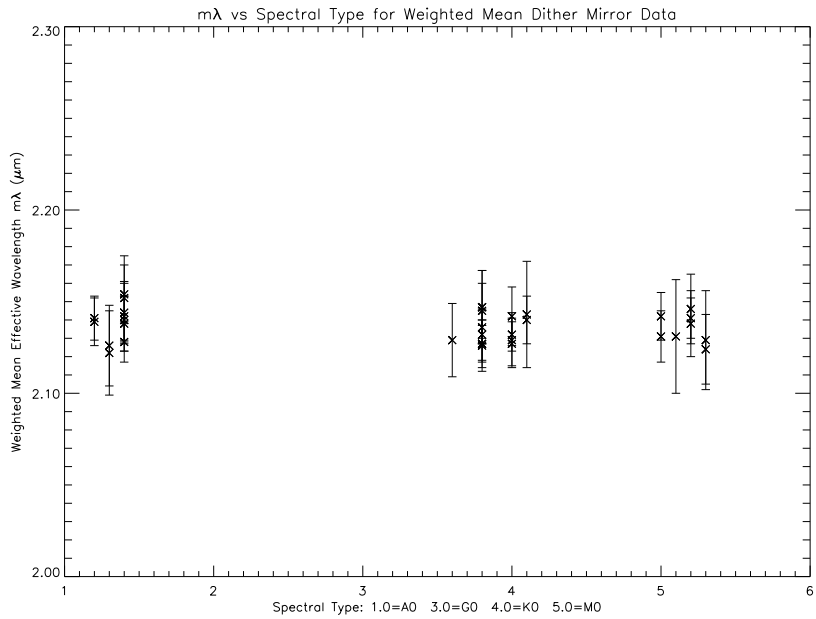

Figure 4.9: Weighted mean effective wavelength versus spectral type for dither data. The $m\lambda$ values used are the weighted mean of the results from all data sets for that star on the same night. No change in effective wavelength is detected with a change in object temperature. The objects are plotted by decreasing temperature based on their spectral type with AFGKM representing 12345 respectively. The A2 stars are plotted at 1.2, the G6 stars are plotted at 3.6, K0 stars at 4.0, M1 stars at 5.1, and so on.

slightly lower than the OPLE cart result, but not by enough to be relevant. The reduced χ^2 value for all 224 dither data sets analyzed together is extremely low (0.11), indicating that the error estimate is still significantly too large.

4.3 Comparing OPLE Cart and Dither Mirror Results

The weighted mean effective wavelength results for the two data collection methods are very similar, while the weighted mean bandwidth values differ by almost 5% (Figure 4.11). We do not have an explanation for the large discrepancy in the measured passband widths.

We cannot judge whether one method is more suited to measuring the effective wavelength than the other. Owing to the fact that we do not find one effective wavelength measurement

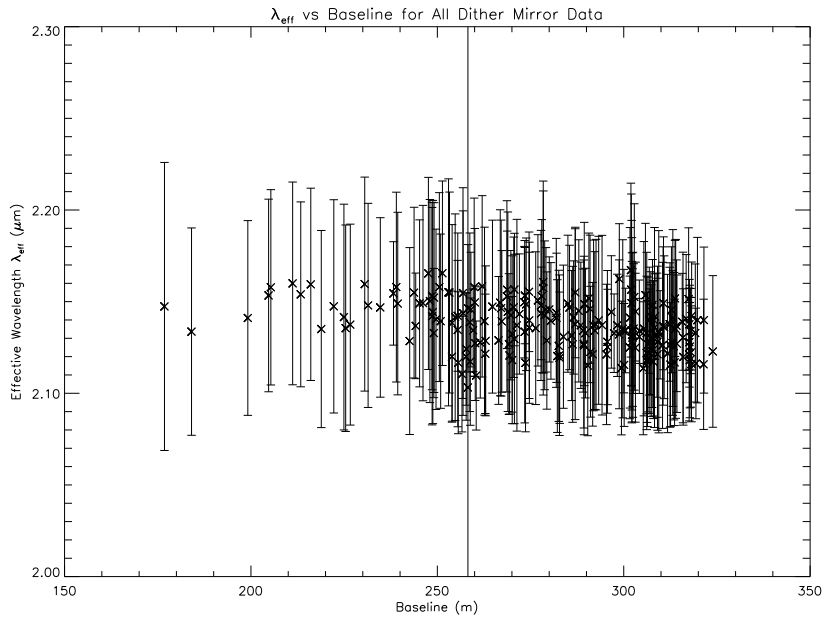

Figure 4.10: Effective wavelength versus baseline length for all observations collected using the dither mirror. No change in the effective wavelength is detected with the change in baseline length. The error bar that goes off the plot has a value of $0.553\mu m$ and belongs to data set 8 of the HD 114093 observations from 2008_04_21.

more valid than the other, we choose to adopt $2.138 \pm 0.003\mu m$, an average of the two results, as our best estimate of the K'-band effective wavelength of CHARA Classic.

Table 4.3: Overall Weighted Mean Results.

Fringe Scan Method	**N**	$\overline{\lambda_{eff}}$ (μm)	$\overline{\sigma\lambda_{eff}}$ (%)	χ^2_ν	$\overline{\Delta\lambda}$ (μm)
OPLE Cart	61	2.140 ± 0.003	0.14	0.99	0.334 ± 0.002
Dither Mirror	224	2.136 ± 0.002	0.09	0.11	0.351 ± 0.003

NOTES.— The weighted mean effective wavelength and bandwidth for all OPLE cart data sets and the weighted mean effective wavelength and bandwidth for all dither mirror data sets. The reduced χ^2 (χ^2_ν) value is calculated from the individual data sets from that star on that night.

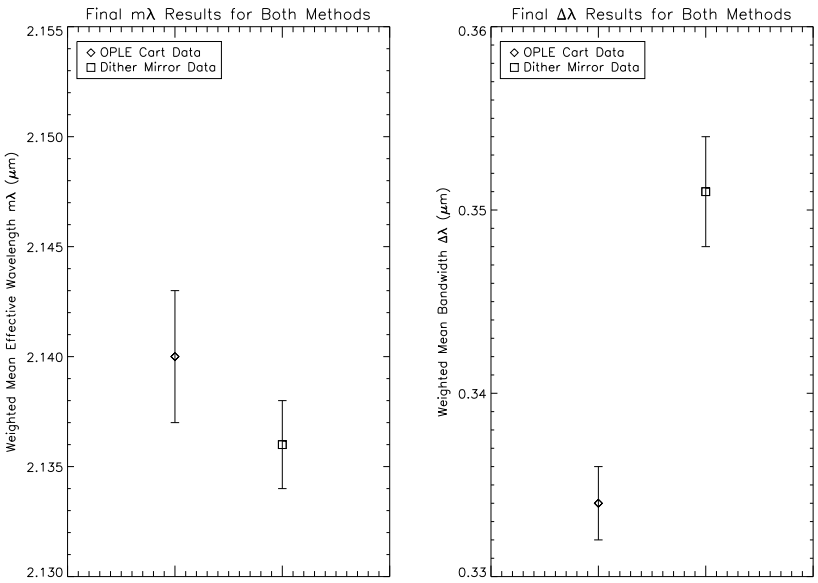

Figure 4.11: Effective wavelength (left) and bandwidth (right) results for the two observing methods. Both plots use the weighted mean value of all data sets collected using the same method.

It should be noted that the CHARA Classic beam combiner went through some slight changes in 2009 April, between the time when the dither mirror data were collected and the time with the OPLE cart data were collected. The optical path carrying the beam combiner outputs to the detector changed. At our level of precision, we do not think this modification impacted our results.

4.4 Comparing Measured and Modeled Effective Wavelengths

Both empirically measured effective wavelength results presented in this thesis are less than the previously accepted effective wavelength value derived from the model (see Section 1.4 and Figure 1.2). Interestingly, the effective wavelength values measured using the OPLE cart and the dither mirror are both closer to the centroid wavelength of the actual K' filter transmission measured by the manufacturer (the middle solid vertical line in Figure 1.2).

Table 4.4 and Figure 4.12 show our results compared with the modeled effective wavelength and the peak transmission of the K' filter.

Table 4.4: Measured effective wavelength results compared with previous values.

Type	$\lambda_{eff}(\mu m)$
K' peak transmission	2.1398
Modeled	2.1501
Measured (OPLE cart)	2.140 ± 0.003
Measured (dither mirror)	2.136 ± 0.002

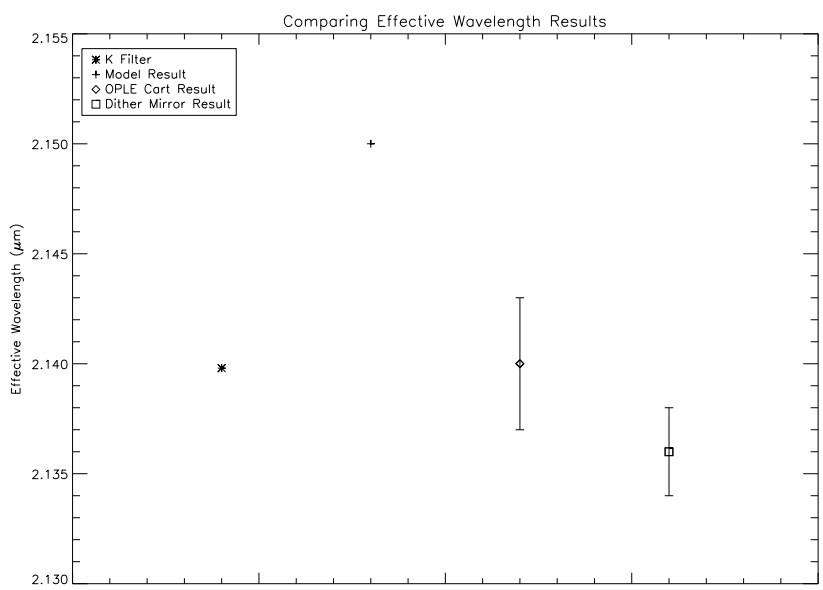

Figure 4.12: Comparing effective wavelength results with previous values. The overall weighted mean results for both methods (Figure 4.11) are shown with the modeled effective wavelength and the peak transmission wavelength for the K' filter.

We expected our measured effective wavelength values to be more similar to the modeled effective wavelength value. The proximity of our results to the peak transmission wavelength

of the filter indicates an inaccuracy in the implementation of the model. The model does not properly account for the factors that affect the wavelength of light observed, including the Earth's atmosphere and the optical surfaces along the light path (Section 1.3-1.4). Unfortunately, we cannot use our measured value to refine the model because there are too many factors impacting the effective wavelength. Our measured effective wavelength values do not indicate exactly where the inadequacies of the model lie.

– 5 –

Future Work

5.1 CHARA Classic Rebuild

CHARA Classic has been undergoing modifications to expand it from a two-way beam combiner into a three-way beam combiner. The first phase of changes occurred in 2009 April, between the time when the dither mirror data were collected and the time when the OPLE cart data were collected. These modifications included changing the way the outputs from the beam combiner travel into the infrared camera.

The second phase of changes occurred this year and could potentially have an impact on the effective wavelength value. During phase two, additional optics were installed to enable the use of three beams instead of only two.

If we were to perform this project again with the reconfigured CHARA Classic, it is not known whether our results would be different. It is possible that our level of precision is not sufficient to detect the change. The only way to know for sure is to perform the experiment again and collect data using the new CHARA Classic.

As discussed in Section 4, our level of precision in the measured effective wavelength value did not vary drastically between the data collected using the dither mirror to scan through the fringes and the data collected using the OPLE cart for fringe scanning. Perhaps a good way to get an idea of whether we can detect a change in the effective wavelength due to the Classic rebuild is to analyze data collected with the dither mirror for standard observing purposes during the Summer 2010 and Fall 2010 observing seasons. This approach means that we would not need dedicated time on the Array to collect data specifically for the purpose of measuring the effective wavelength. We would analyze this new dither mirror

data the same way we did previously (see Section 3.3). If the new results differ from the dither mirror results prior to the CHARA Classic rebuild, then we know we should perform a more extensive effective wavelength measurement. We can then work on collecting data using the OPLE carts to scan through the interference fringes.

5.2 Another Approach to Measuring the Effective Wavelength

The NPOI regularly conducts white light observations to make measurements of their effective wavelength (Hutter, D. J. 2010, private communication). The white light is set up in the lab, so data collected in this way do not include the effects of the entire optical path on the light from a star. Rather, the data only captures attenuations of the light due to effects in the lab. Changes in the wavelength of observed light due to the atmosphere, optical surfaces encountered in the telescopes, and optical surfaces encountered in the tubes carrying the light into the lab are not captured. NPOI is able to conduct these observations frequently because the set up is in the lab and easily accessible anytime the array is not being used for other purposes. By collecting these data regularly for an extended period of time, they can detect changes in the effective wavelength over time.

Even though the observations are not along the entire light path, they are still better than nothing. One could argue the fact that there are many observations taken frequently offsets the negative aspect of the observations only including part of the light path.

Developing a similar setup for the CHARA Array could be beneficial. There is already a white light source installed in the lab, but we do not know how well the existing source performs at the relevant infrared wavelengths. It is definitely worth investigating implement-

ing this approach on the CHARA Array. We could potentially easily and regularly make effective wavelength measurements for all of the CHARA beam combiners.

– 6 –

Conclusion

We empirically measured the effective wavelength of CHARA Classic's K' filter using two observational methods. We used data collected using the OPLE cart to scan through the interference fringes and data collected using the dither mirror to scan through the fringes. We measure an overall effective wavelength of $2.140 \pm 0.003\mu m$ with the OPLE cart method and $2.136 \pm 0.002\mu m$ with the dither mirror method. Based upon these results, we adopt a value of $2.138 \pm 0.003\mu m$ as the best estimate for the K'-band effective wavelength of the CHARA Classic beam combiner.

At our level of precision, target temperature and elevation angle do not impact the effective wavelength value. Both of our measured effective wavelength values are more similar to the actual wavelength of light transmitted by the K' filter ($2.1398\mu m$) than they are to the previous value of the effective wavelength ($2.150\mu m$) derived from a model of the system.

Shifting from the previous effective wavelength value to our newly adopted value of $2.138 \pm 0.003\mu m$ represents a decrease of just over 0.5%. From Table 1.1, one can calculate that a 0.5% change in effective wavelength causes an average 0.45σ change in the measured uniform disk angular diameter. The new effective wavelength value will result in smaller angular diameter values by 0.45σ on average.

References

Baines, E. K., McAlister, H. A., ten Brummelaar, T. A., Sturmann, J., Sturmann, L., Turner, N. H., & Ridgway, S. T. 2009, ApJ, 701, 154

Benson, J. A., Dyck, H. M., & Howell, R. R. 1995, Appl. Opt., 34, 51

Berger, D. H., et al. 2006, ApJ, 644, 475

Boyajian, T. S., et al. 2008, ApJ, 683, 424

Carroll, B. W., & Ostlie, D. A. 1996, An Introduction to Modern Astrophysics (Reading, MA: Addison-Wesley)

Coude Du Foresto, V., Ridgway, S., & Mariotti, J. 1997, A&AS, 121, 379

Kitchin, C. R. 2003, Astrophysical Techniques, 4th edn. (Bristol; Philadelphia: Institute of Physics Publishing)

ten Brummelaar, T. A., et al. 2005, ApJ, 628, 453

Appendices

– **A** –

Appendix A: OPLE Cart Data

This appendix includes detailed tables of the data taken using the OPLE carts to scan through the interference fringes. The results are broken down into three different tables, one for each star. The tables here are more detailed versions of Table 4.1. As previously mentioned, the mean effective wavelength and bandwidth values presented in Table 4.1 are weighted averages of the results from all data sets taken of the same star in one night. Here in Tables A.1, A.2, A.3, we list the results from each data set separately and do not present any weighted mean values. Also note that the observation dates here are given in MJD, while they are presented in UT in Table 4.1.

The mean effective wavelength (λ_{eff}) and bandwidth ($\Delta\lambda$) values are given for each data set along with their associated errors ($\sigma\lambda_{eff}$, $\sigma\Delta\lambda$). The eighth column contains the measurement of the baseline in the middle of each observation while the ninth column gives by how many meters the length of the baseline changed during the course of that observation. The tenth and eleventh columns include the altitude and azimuth of the star in the middle of each observation.

Please note that while the data in Appendix B were collected using several different telescope pairs, all of the data presented in Appendix A were collected using telescopes S1 and S2.

Table A.1: Results from each data set of the OPLE cart data for HD 102647.

HD 102647									
Seq #	**Obs Date** (JD)	λ_{eff} (μm)	$\sigma\lambda_{eff}$ (μm)	$\Delta\lambda$ (μm)	$\sigma\Delta\lambda$ (μm)	**Baseline** (m)	**Baseline range** (m)	**Alt** (°)	**Az** (°)
1	54970.674	2.122	0.043	0.328	0.023	32.5030	0.0127	70.0	11.9
2	54970.676	2.109	0.049	0.342	0.030	32.5318	0.0125	69.8	14.0
3	54970.678	2.172	0.081	0.341	0.030	32.5605	0.0128	69.7	16.0
4	54970.683	2.128	0.054	0.342	0.026	32.6323	0.0144	69.2	20.8
5	54970.685	2.149	0.050	0.343	0.026	32.6648	0.0141	69.0	22.8
6	54970.687	2.161	0.055	0.336	0.020	32.6965	0.0138	68.7	24.7
7	54970.689	2.150	0.052	0.340	0.026	32.7277	0.0140	68.5	26.5
1	54983.666	2.133	0.021	0.332	0.015	32.9254	0.0199	66.5	36.6
2	54983.668	2.112	0.028	0.333	0.011	32.9660	0.0166	66.1	38.4
3	54983.671	2.129	0.035	0.334	0.019	33.0021	0.0166	65.7	40.0
4	54983.673	2.109	0.040	0.329	0.016	33.0382	0.0161	65.2	41.5
5	54983.675	2.131	0.019	0.334	0.009	33.0779	0.0207	64.8	43.1
6	54983.678	2.144	0.036	0.333	0.016	33.1191	0.0173	64.2	44.8
7	54983.681	2.140	0.037	0.334	0.019	33.1761	0.0361	63.5	46.9
8	54983.685	2.131	0.022	0.334	0.011	33.2360	0.0211	62.7	49.1
9	54983.687	2.131	0.029	0.339	0.014	33.2780	0.0170	62.1	50.5
10	54983.690	2.126	0.033	0.335	0.014	33.3193	0.0213	61.5	51.9
11	54983.692	2.111	0.026	0.335	0.017	33.3586	0.0145	61.0	53.2
12	54983.695	2.126	0.020	0.331	0.008	33.4005	0.0242	60.3	54.6
13	54983.698	2.131	0.041	0.334	0.018	33.4425	0.0141	59.7	55.9
14	54983.700	2.115	0.017	0.329	0.009	33.4796	0.0192	59.1	57.1
15	54983.702	2.126	0.018	0.334	0.009	33.5145	0.0136	58.5	58.1
16	54983.705	2.128	0.025	0.330	0.011	33.5482	0.0165	57.9	59.2
17	54983.707	2.135	0.030	0.331	0.016	33.5815	0.0142	57.3	60.2
18	54983.709	2.125	0.025	0.326	0.010	33.6138	0.0149	56.8	61.1

Table A.2: Results from each data set of the OPLE cart data for HD 119850.

HD 119850									
Seq #	**Obs Date** (JD)	λ_{eff} (μm)	$\sigma\lambda_{eff}$ (μm)	$\Delta\lambda$ (μm)	$\sigma\Delta\lambda$ (μm)	**Baseline** (m)	**Baseline range** (m)	**Alt** (°)	**Az** (°)
1	54983.721	2.158	0.037	0.325	0.023	32.5722	0.0191	70.2	13.2

Continued on next page

Table A.2 – continued from previous page

HD 119850 (con't)									
Seq #	**Obs Date** (JD)	λ_{eff} (μm)	$\sigma\lambda_{eff}$ (μm)	$\Delta\lambda$ (μm)	$\sigma\Delta\lambda$ (μm)	**Baseline** (m)	**Baseline range** (m)	**Alt** (°)	**Az** (°)
2	54983.725	2.119	0.020	0.331	0.020	32.6333	0.0346	69.9	17.5
3	54983.729	2.134	0.029	0.329	0.010	32.6980	0.0187	69.4	21.9
4	54983.733	2.118	0.014	0.331	0.016	32.7429	0.0181	69.1	24.7
5	54983.735	2.147	0.020	0.334	0.017	32.7842	0.0153	68.7	27.2
6	54983.738	2.142	0.030	0.344	0.026	32.8263	0.0198	68.3	29.6
7	54983.741	2.135	0.047	0.328	0.019	32.8755	0.0217	67.8	32.2
8	54983.744	2.133	0.022	0.344	0.014	32.9222	0.0159	67.3	34.6
9	54983.747	2.149	0.039	0.341	0.014	32.9628	0.0172	66.9	36.6
10	54983.749	2.123	0.023	0.330	0.017	33.0034	0.0156	66.4	38.5
11	54983.752	2.151	0.013	0.344	0.010	33.0426	0.0168	66.0	40.3
12	54983.754	2.138	0.020	0.331	0.015	33.0827	0.0157	65.5	42.0
13	54983.757	2.152	0.015	0.347	0.017	33.1234	0.0174	65.0	43.7
14	54983.760	2.124	0.036	0.326	0.018	33.1754	0.0269	64.3	45.8
15	54983.763	2.144	0.033	0.336	0.022	33.2312	0.0184	63.6	47.9

Table A.3: Results from each data set of the OPLE cart data for HD 131156.

HD 131156									
Seq #	**Obs Date** (JD)	λ_{eff} (μm)	$\sigma\lambda_{eff}$ (μm)	$\Delta\lambda$ (μm)	$\sigma\Delta\lambda$ (μm)	**Baseline** (m)	**Baseline range** (m)	**Alt** (°)	**Az** (°)
1	54970.737	2.109	0.054	0.325	0.027	32.8747	0.0008	67.7	308.0
2	54970.739	2.177	0.044	0.338	0.019	32.8739	0.0002	68.1	309.1
3	54970.741	2.122	0.041	0.324	0.023	32.8738	0.0002	68.6	310.7
4	54970.744	2.116	0.027	0.339	0.022	32.8749	0.0008	69.2	312.4
5	54970.747	2.176	0.030	0.350	0.027	32.8777	0.0017	69.8	314.6
6	54970.748	2.148	0.026	0.343	0.025	32.8799	0.0014	70.1	315.9
7	54970.750	2.161	0.048	0.327	0.023	32.8837	0.0018	70.6	317.6
1	54983.777	2.127	0.029	0.330	0.013	33.3111	0.0229	73.2	28.0
2	54983.780	2.135	0.054	0.331	0.021	33.3507	0.0124	72.6	31.8
3	54983.782	2.151	0.048	0.330	0.020	33.3791	0.0122	72.2	34.4
4	54983.786	2.135	0.024	0.338	0.011	33.4116	0.0166	71.7	37.2
5	54983.789	2.143	0.033	0.332	0.014	33.4459	0.0143	71.1	40.0
6	54983.791	2.146	0.019	0.335	0.009	33.4760	0.0121	70.6	42.2
7	54983.794	2.120	0.025	0.330	0.010	33.5071	0.0152	70.0	44.5

Continued on next page

Table A.3 – continued from previous page

HD 131156 (con't)									
Seq #	**Obs Date** (JD)	λ_{eff} (μm)	$\sigma\lambda_{eff}$ (μm)	$\Delta\lambda$ (μm)	$\sigma\Delta\lambda$ (μm)	**Baseline** (m)	**Baseline range** (m)	**Alt** (°)	**Az** (°)
8	54983.797	2.138	0.027	0.333	0.013	33.5370	0.0113	69.5	46.5
9	54983.800	2.155	0.031	0.339	0.013	33.5692	0.0170	68.8	48.6
10	54983.803	2.147	0.025	0.334	0.018	33.6062	0.0157	68.1	50.9
11	54983.806	2.121	0.030	0.336	0.015	33.6402	0.0148	67.4	52.9
12	54983.809	2.123	0.013	0.334	0.009	33.6709	0.0127	66.7	54.7
13	54983.811	2.194	0.009	0.344	0.009	33.6988	0.0118	66.0	56.2
14	54983.814	2.127	0.020	0.338	0.013	33.7249	0.0109	65.4	57.6

– **B** –

Appendix B: Dither Mirror Data

This appendix includes a detailed table of the data taken using the dither mirror to scan through the interference fringes. The table here is a more detailed version of Table 4.2. As previously mentioned, the mean effective wavelength and bandwidth values presented in Table 4.2 are weighted averages of the results from all data sets taken of the same star in one night. Here in Table B.1, we list the results from each data set separately and do not present any weighted mean values. Also note that the observation dates in Table 4.2 are listed in UT and in Table B.1 they are presented in MJD.

The mean effective wavelength (λ_{eff}) and bandwidth ($\Delta\lambda$) values are given for each data set along with their associated errors ($\sigma\lambda_{eff}$, $\sigma\Delta\lambda$). The eighth column contains the measurement of the baseline in the middle of each observation while the ninth column gives by how many meters the length of the baseline changed during the course of that observation. The tenth and eleventh columns include the altitude and azimuth of the star in the middle of each observation. The dither mirror data were taken using many different pairs of telescopes, therefore the telescopes used for each data set are listed in the last column of the table.

Table B.1: Results from each data set of the dither mirror data.

HD	**Seq #**	**Obs Date** (MJD)	λ_{eff} (μm)	$\sigma\lambda_{eff}$ (μm)	$\Delta\lambda$ (μm)	$\sigma\Delta\lambda$ (μm)	**Baseline** (m)	**Baseline range** (m)	**Alt** (°)	**Az** (°)	**Telescopes used**
71	1	54763.683	2.133	0.021	0.343	0.014	297.4099	0.2072	64.2	207.4	W1-E1
...	2	54763.692	2.134	0.023	0.349	0.025	300.4986	0.1868	65.4	204.0	...
...	3	54763.701	2.145	0.027	0.338	0.027	303.1963	0.1664	66.4	200.2	...
...	4	54763.705	2.134	0.018	0.335	0.020	304.2896	0.1572	66.8	198.5	...
...	5	54763.713	2.117	0.033	0.335	0.038	306.2442	0.1392	67.4	194.8	...
...	6	54763.720	2.117	0.030	0.332	0.030	307.9524	0.1212	67.9	190.9	...
...	7	54763.730	2.132	0.024	0.335	0.037	309.7499	0.0990	68.4	185.7	...
1326	1	54725.894	2.140	0.043	0.372	0.065	301.6858	0.0158	75.0	135.0	E1-S2
...	2	54725.906	2.167	0.047	0.409	0.084	301.9281	0.0104	72.4	129.4	...
...	3	54725.913	2.157	0.052	0.455	0.103	302.0362	0.0078	70.6	126.8	...
...	4	54725.921	2.149	0.045	0.373	0.070	302.1202	0.0055	68.7	124.7	...
...	5	54725.928	2.134	0.051	0.389	0.071	302.1737	0.0039	66.9	123.2	...
...	6	54725.935	2.134	0.043	0.371	0.068	302.2114	0.0027	65.1	122.1	...
1326	1	54726.717	2.137	0.047	0.348	0.055	291.9098	0.3236	52.1	240.4	E1-S1
...	2	54726.725	2.128	0.039	0.340	0.035	295.6320	0.3027	54.0	240.4	...
...	3	54726.731	2.162	0.030	0.352	0.033	298.8325	0.2839	55.7	240.4	...
...	4	54726.738	2.125	0.039	0.336	0.036	301.6550	0.2666	57.4	240.2	...
...	5	54726.748	2.154	0.039	0.356	0.046	305.8317	0.2396	60.1	239.8	...
...	6	54726.761	2.137	0.043	0.346	0.033	310.5673	0.2066	63.5	238.7	...
...	7	54726.767	2.126	0.045	0.340	0.033	312.4031	0.1930	64.9	238.0	...
...	8	54726.773	2.137	0.036	0.349	0.041	314.1776	0.1793	66.4	237.1	...
...	9	54726.779	2.130	0.047	0.347	0.042	315.8974	0.1655	68.0	236.0	...
...	10	54726.785	2.151	0.039	0.349	0.041	317.4119	0.1529	69.4	234.6	...
...	11	54726.796	2.140	0.045	0.347	0.040	319.7752	0.1321	71.9	231.4	...
...	12	54726.804	2.140	0.040	0.345	0.042	321.5144	0.1157	73.9	227.7	...

Continued on next page

Table B.1 – continued from previous page

HD	Seq #	Obs Date (MJD)	λ_{eff} (μm)	$\sigma\lambda_{eff}$ (μm)	$\Delta\lambda$ (μm)	$\sigma\Delta\lambda$ (μm)	Baseline (m)	Baseline range (m)	Alt (°)	Az (°)	Telescopes used
1326	1	54762.747	2.138	0.031	0.367	0.053	312.3347	0.0742	80.1	187.9	W1-E1
...	2	54762.756	2.141	0.048	0.372	0.060	313.1725	0.0396	80.1	174.0	...
...	3	54762.772	2.126	0.040	0.347	0.040	313.4511	0.0169	78.8	152.8	...
...	4	54762.783	2.146	0.034	0.345	0.048	312.7924	0.0549	76.9	141.8	...
9407	1	54741.737	2.120	0.042	0.349	0.036	282.1850	0.1762	47.2	202.1	W1-E1
...	2	54741.752	2.127	0.043	0.346	0.030	286.2966	0.1551	48.9	200.4	...
...	3	54741.770	2.146	0.040	0.356	0.036	290.9655	0.1480	50.7	198.1	...
...	4	54741.788	2.121	0.038	0.358	0.040	295.3841	0.1372	52.2	195.2	...
26965	1	54762.826	2.140	0.046	0.363	0.073	293.2739	0.4548	38.1	317.5	W1-E1
...	2	54762.843	2.153	0.051	0.372	0.083	302.8331	0.3020	41.2	324.1	...
...	3	54762.856	2.136	0.055	0.377	0.092	308.2561	0.2258	43.4	329.7	...
26965	1	54763.798	2.153	0.026	0.334	0.021	273.4905	0.5259	32.5	308.6	W1-E1
...	2	54763.806	2.139	0.032	0.331	0.019	280.4650	0.4837	34.4	311.3	...
...	3	54763.814	2.141	0.031	0.334	0.025	286.5563	0.4413	36.1	314.0	...
...	4	54763.835	2.134	0.034	0.327	0.022	300.0587	0.3187	40.2	321.9	...
...	5	54763.843	2.131	0.031	0.315	0.023	304.1744	0.2674	41.7	325.3	...
...	6	54763.855	2.132	0.034	0.326	0.033	308.9303	0.1889	43.7	330.6	...
36395	1	54762.893	2.135	0.049	0.384	0.080	299.7310	0.3655	44.1	320.2	W1-E1
...	2	54762.934	2.127	0.039	0.367	0.073	313.1278	0.0722	50.3	340.0	...
79211	1	54761.945	2.137	0.029	0.334	0.027	244.2024	0.4373	41.0	226.9	E1-S1
...	2	54761.958	2.120	0.036	0.339	0.034	253.9386	0.4045	44.0	227.1	...
...	3	54761.972	2.122	0.033	0.333	0.033	262.8820	0.3719	46.9	227.1	...
...	4	54761.983	2.121	0.032	0.349	0.049	269.3835	0.3670	49.3	226.8	...
...	5	54761.998	2.144	0.025	0.349	0.028	277.8479	0.3112	52.5	226.1	...
79211	1	54763.956	2.154	0.028	0.336	0.021	238.2412	0.3698	44.5	227.1	W1-E1
...	2	54763.973	2.133	0.035	0.334	0.025	249.0640	0.3941	48.3	227.0	...
...	3	54763.995	2.129	0.041	0.341	0.027	262.9721	0.3566	53.1	225.9	...
...	4	54764.013	2.150	0.030	0.350	0.021	273.3460	0.3320	56.9	224.1	...

Continued on next page

Table B.1 – continued from previous page

HD	Seq #	Obs Date (MJD)	λ_{eff} (μm)	$\sigma\lambda_{eff}$ (μm)	$\Delta\lambda$ (μm)	$\sigma\Delta\lambda$ (μm)	Baseline (m)	Baseline range (m)	Alt (°)	Az (°)	Telescopes used
...	5	54764.025	2.146	0.029	0.349	0.021	280.0288	0.3100	59.4	222.3	...
...	6	54764.037	2.131	0.035	0.352	0.027	286.0303	0.2855	61.7	220.0	...
...	7	54764.051	2.134	0.043	0.356	0.034	292.2379	0.2545	64.2	216.6	...
102124	1	54575.647	2.154	0.050	0.428	0.106	213.3560	0.2766	49.5	302.0	W1-S1
...	2	54575.654	2.159	0.052	0.448	0.104	216.0546	0.3004	51.2	304.7	...
...	3	54575.668	2.147	0.058	0.489	0.142	222.2288	0.3390	54.5	310.9	...
...	4	54575.677	2.137	0.055	0.423	0.089	226.6468	0.3566	56.5	315.5	...
...	5	54575.685	2.160	0.058	0.539	0.200	230.5169	0.3665	58.1	319.8	...
...	6	54575.693	2.147	0.049	0.421	0.081	234.7005	0.3723	59.6	324.6	...
...	7	54575.703	2.149	0.050	0.529	0.170	239.3774	0.3733	61.0	330.5	...
...	8	54575.711	2.155	0.047	0.437	0.106	243.7580	0.3693	62.2	336.5	...
...	9	54575.719	2.165	0.052	0.409	0.067	247.6006	0.3618	63.0	342.2	...
...	10	54575.726	2.165	0.050	0.465	0.105	251.3648	0.3509	63.6	348.1	...
102124	1	54578.660	2.123	0.041	0.354	0.055	323.9042	0.2027	54.6	311.1	E1-S1
...	2	54578.670	2.116	0.036	0.345	0.043	321.4284	0.2302	56.6	315.8	...
...	3	54578.678	2.133	0.038	0.349	0.040	319.1948	0.2498	58.2	320.1	...
...	4	54578.685	2.141	0.035	0.354	0.033	316.7418	0.2670	59.6	324.8	...
...	5	54578.695	2.117	0.034	0.355	0.028	313.6387	0.2835	61.1	330.8	...
...	6	54578.703	2.149	0.036	0.359	0.034	310.6694	0.2946	62.2	336.8	...
...	7	54578.711	2.124	0.038	0.362	0.030	307.9437	0.3012	63.0	342.4	...
...	8	54578.718	2.114	0.036	0.358	0.026	305.2296	0.3045	63.6	348.2	...
...	9	54578.726	2.130	0.038	0.361	0.027	302.3770	0.3045	63.9	354.5	...
...	10	54578.734	2.114	0.036	0.356	0.022	299.3912	0.3007	64.0	1.2	...
...	11	54578.742	2.144	0.031	0.360	0.020	296.6763	0.2936	63.9	7.2	...
114093	1	54577.642	2.153	0.051	0.426	0.125	248.5729	0.0166	42.1	266.0	W1-S1
...	2	54577.651	2.141	0.058	0.467	0.115	248.5902	0.0209	44.7	267.6	...
...	3	54577.657	2.144	0.061	0.539	0.171	248.7925	0.0477	46.6	268.8	...
...	4	54577.670	2.140	0.049	0.490	0.156	249.6401	0.0984	50.3	271.4	...

Continued on next page

Table B.1 – continued from previous page

HD	Seq #	Obs Date (MJD)	λ_{eff} (μm)	$\sigma\lambda_{eff}$ (μm)	$\Delta\lambda$ (μm)	$\sigma\Delta\lambda$ (μm)	Baseline (m)	Baseline range (m)	Alt (°)	Az (°)	Telescopes used
...	5	54577.681	2.139	0.048	0.503	0.153	250.8947	0.1408	53.6	273.9	...
...	6	54577.695	2.155	0.062	0.500	0.148	253.0007	0.1861	57.7	277.2	...
...	7	54577.708	2.135	0.053	0.495	0.154	255.4816	0.2347	61.6	280.9	...
...	8	54577.720	2.103	0.553	0.479	0.315	255.4816	0.2347	65.2	285.1	...
...	9	54577.727	2.158	0.049	0.461	0.138	259.8744	0.2372	67.3	288.0	...
...	10	54577.738	2.139	0.051	0.412	0.093	256.6615	0.2110	70.5	293.6	...
...	11	54577.747	2.147	0.047	0.398	0.088	264.8224	0.2444	72.9	298.9	...
...	12	54577.756	2.149	0.051	0.410	0.303	266.8842	0.2397	75.0	305.3	...
...	13	54577.764	2.144	0.054	0.433	0.138	268.9082	0.2304	77.0	313.7	...
114093	1	54644.689	2.122	0.030	0.346	0.029	317.9899	0.0241	63.5	77.0	E1-S1
...	2	54644.697	2.125	0.034	0.343	0.034	317.7279	0.0135	61.1	79.6	...
...	3	54644.704	2.138	0.025	0.340	0.028	317.6232	0.0046	59.1	81.5	...
...	4	54644.710	2.128	0.025	0.349	0.030	317.6168	0.0033	57.3	83.1	...
...	5	54644.718	2.118	0.032	0.344	0.037	317.7397	0.0142	54.9	85.2	...
...	6	54644.725	2.134	0.023	0.343	0.026	317.9274	0.0221	53.1	86.6	...
...	7	54644.730	2.115	0.032	0.348	0.040	318.1787	0.0293	51.3	87.9	...
131156	1	54574.861	2.146	0.048	0.372	0.057	267.1147	0.1705	74.4	344.9	W1-S1
...	2	54574.874	2.130	0.046	0.370	0.051	270.6758	0.1495	74.9	1.7	...
...	3	54574.914	2.148	0.041	0.363	0.042	277.7999	0.0505	69.8	45.2	...
...	4	54574.925	2.161	0.050	0.427	0.102	278.4223	0.0193	67.4	52.9	...
...	5	54574.943	2.153	0.042	0.363	0.045	278.0200	0.0442	62.8	62.7	...
131156	1	54575.779	2.129	0.051	0.401	0.069	242.5792	0.1776	57.2	289.0	W1-S1
...	2	54575.792	2.149	0.053	0.431	0.108	246.1465	0.2734	60.8	294.0	...
...	3	54575.802	2.152	0.052	0.412	0.108	249.1229	0.2701	63.4	298.4	...
...	4	54575.806	2.158	0.052	0.385	0.068	250.5349	0.2648	64.6	300.7	...
...	5	54575.817	2.138	0.054	0.450	0.116	253.9665	0.2956	67.2	306.8	...
...	6	54575.826	2.144	0.056	0.433	0.108	256.9022	0.2973	69.3	312.8	...
...	7	54575.842	2.158	0.049	0.444	0.121	262.0177	0.2987	72.3	326.3	...

Continued on next page

Table B.1 – continued from previous page

HD	Seq #	Obs Date (MJD)	λ_{eff} (μm)	$\sigma\lambda_{eff}$ (μm)	$\Delta\lambda$ (μm)	$\sigma\Delta\lambda$ (μm)	Baseline (m)	Baseline range (m)	Alt (°)	Az (°)	Telescopes used
131156	1	54644.751	2.140	0.021	0.345	0.023	308.1298	0.0526	63.1	62.2	E1-S1
...	2	54644.757	2.121	0.028	0.343	0.020	307.6092	0.0411	61.3	65.2	...
...	3	54644.764	2.130	0.031	0.340	0.020	307.2324	0.0296	59.6	67.8	...
...	4	54644.769	2.119	0.030	0.339	0.026	306.9946	0.0187	58.0	70.0	...
...	5	54644.775	2.128	0.029	0.342	0.022	306.8660	0.0079	56.4	72.0	...
...	6	54644.782	2.140	0.029	0.347	0.034	306.8484	0.0055	54.5	74.2	...
...	7	54644.796	2.142	0.024	0.347	0.026	307.2800	0.0313	50.5	78.3	...
...	8	54644.803	2.148	0.025	0.347	0.029	307.7187	0.0438	48.5	80.1	...
...	9	54644.810	2.142	0.023	0.351	0.030	308.3771	0.0571	46.2	82.1	...
140775	1	54669.672	2.149	0.037	0.358	0.043	285.0203	0.3079	60.3	15.7	E1-S1
...	2	54669.681	2.144	0.041	0.360	0.047	281.9093	0.2868	59.5	21.7	...
...	3	54669.688	2.129	0.037	0.358	0.046	279.3736	0.2646	58.6	26.7	...
...	4	54669.696	2.151	0.036	0.361	0.043	276.9770	0.2380	57.4	31.6	...
...	5	54669.705	2.140	0.043	0.370	0.057	274.6649	0.2052	56.0	36.6	...
...	6	54669.709	2.117	0.038	0.355	0.046	273.6564	0.1877	55.2	39.0	...
...	7	54669.717	2.143	0.033	0.354	0.047	272.0088	0.1528	53.6	43.1	...
...	8	54669.726	2.157	0.031	0.357	0.046	270.6861	0.1146	51.9	47.1	...
...	9	54669.734	2.143	0.035	0.357	0.054	269.7207	0.0731	50.0	50.9	...
...	10	54669.742	2.127	0.038	0.360	0.060	269.2141	0.0335	48.1	54.1	...
141795	1	54669.677	2.138	0.033	0.361	0.035	298.7280	0.2993	59.3	15.9	E1-S1
...	2	54669.684	2.146	0.036	0.360	0.030	301.5145	0.3038	58.6	21.1	...
...	3	54669.692	2.132	0.040	0.354	0.034	304.4410	0.3048	57.6	26.2	...
...	4	54669.701	2.150	0.037	0.362	0.029	307.4198	0.3020	56.5	31.1	...
...	5	54669.713	2.114	0.036	0.347	0.033	311.9814	0.2902	54.3	38.3	...
...	6	54669.721	2.156	0.030	0.357	0.033	314.7775	0.2780	52.7	42.4	...
...	7	54669.729	2.135	0.040	0.350	0.032	317.3550	0.2631	51.1	46.2	...
...	8	54669.738	2.127	0.037	0.353	0.035	319.9673	0.2435	49.2	50.0	...
145607	1	54575.858	2.147	0.079	0.423	0.102	176.7987	0.7430	41.3	326.8	W1-S1

Continued on next page

Table B.1 – continued from previous page

HD	Seq #	Obs Date (MJD)	λ_{eff} (μm)	$\sigma\lambda_{eff}$ (μm)	$\Delta\lambda$ (μm)	$\sigma\Delta\lambda$ (μm)	Baseline (m)	Baseline range (m)	Alt (°)	Az (°)	Telescopes used
...	2	54575.867	2.134	0.057	0.410	0.091	184.0611	0.7356	42.7	330.7	...
...	3	54575.885	2.141	0.053	0.411	0.079	199.1625	0.7458	45.0	339.1	...
...	4	54575.892	2.158	0.053	0.427	0.092	205.3413	0.7397	45.7	342.8	...
...	5	54575.909	2.135	0.054	0.420	0.083	218.8660	0.6810	46.8	351.3	...
...	6	54575.918	2.135	0.056	0.421	0.079	225.4054	0.7633	47.1	355.7	...
...	7	54575.937	2.158	0.052	0.405	0.074	239.0032	0.6154	47.1	5.5	...
...	8	54575.946	2.149	0.046	0.402	0.067	245.2398	0.5519	46.7	10.5	...
...	9	54575.962	2.142	0.056	0.391	0.116	254.7835	0.5333	45.5	18.6	...
...	10	54575.969	2.139	0.049	0.390	0.087	258.7187	0.4382	44.7	22.1	...
...	11	54575.992	2.153	0.052	0.438	0.131	268.6623	0.3890	41.6	32.5	...
...	12	54576.000	2.137	0.058	0.413	0.118	271.3420	0.2898	40.2	35.8	...
145607	1	54577.886	2.153	0.053	0.421	0.083	204.7374	0.7121	45.7	342.4	W1-S1
...	2	54577.894	2.160	0.059	0.441	0.095	211.1792	0.7291	46.3	346.4	...
...	3	54577.912	2.142	0.062	0.451	0.104	224.9413	0.7918	47.1	355.4	...
...	4	54577.920	2.148	0.056	0.461	0.134	231.4209	0.8846	47.2	179.9	...
...	5	54577.945	2.150	0.055	0.456	0.144	248.0069	0.7022	46.4	12.8	...
...	6	54577.954	2.155	0.055	0.461	0.110	253.2582	0.6268	45.7	17.2	...
145607	1	54578.824	2.126	0.045	0.368	0.063	310.4089	0.4168	36.6	316.9	E1-S1
...	2	54578.833	2.124	0.040	0.363	0.064	306.1635	0.4527	38.4	320.2	...
...	3	54578.840	2.132	0.045	0.373	0.056	302.4782	0.4797	39.7	323.0	...
...	4	54578.859	2.126	0.044	0.359	0.040	291.6648	0.4995	42.8	331.0	...
...	5	54578.867	2.155	0.036	0.374	0.049	287.0031	0.5390	43.8	334.4	...
...	6	54578.886	2.155	0.034	0.358	0.031	274.6094	0.5252	45.9	343.7	...
...	7	54578.893	2.132	0.043	0.356	0.035	270.0783	0.5301	46.4	347.2	...
...	8	54578.908	2.150	0.040	0.358	0.043	260.0499	0.5295	47.1	354.9	...
...	9	54578.915	2.142	0.030	0.354	0.034	255.4474	0.5234	47.2	358.6	...
145607	1	54579.824	2.134	0.055	0.395	0.088	309.3976	0.4259	37.1	317.7	E1-S1
...	2	54579.832	2.135	0.048	0.399	0.074	305.3954	0.4410	38.7	320.7	...

Continued on next page

Table B.1 – continued from previous page

HD	Seq #	Obs Date (MJD)	λ_{eff} (μm)	$\sigma\lambda_{eff}$ (μm)	$\Delta\lambda$ (μm)	$\sigma\Delta\lambda$ (μm)	Baseline (m)	Baseline range (m)	Alt (°)	Az (°)	Telescopes used
...	3	54579.852	2.137	0.049	0.410	0.092	294.1850	0.5289	42.2	329.1	...
...	4	54579.860	2.149	0.045	0.397	0.071	289.4061	0.5510	43.3	332.7	...
...	5	54579.878	2.157	0.058	0.437	0.112	278.4041	0.6314	45.4	340.9	...
...	6	54579.885	2.134	0.050	0.442	0.111	273.4276	0.5726	46.0	344.6	...
...	7	54579.910	2.155	0.057	0.483	0.141	256.8838	0.7086	47.2	357.4	...
158633	1	54668.903	2.152	0.036	0.365	0.053	290.6476	0.1180	40.8	152.5	E1-S1
...	2	54668.911	2.126	0.049	0.353	0.054	289.3382	0.1317	39.6	152.3	...
...	3	54668.920	2.145	0.039	0.379	0.076	287.9466	0.1572	38.4	152.2	...
...	4	54668.925	2.138	0.052	0.349	0.039	286.9770	0.1539	37.7	152.2	...
...	5	54668.933	2.147	0.034	0.348	0.040	285.4627	0.1670	36.6	152.2	...
...	6	54668.941	2.131	0.039	0.342	0.036	283.8109	0.1804	35.5	152.3	...
167564	1	54578.936	2.133	0.044	0.376	0.081	306.1550	0.4824	45.7	323.8	E1-S1
...	2	54578.944	2.128	0.044	0.368	0.089	302.1794	0.5090	47.1	327.5	...
...	3	54578.962	2.137	0.047	0.373	0.075	292.5727	0.4781	49.6	336.6	...
...	4	54578.969	2.137	0.034	0.356	0.067	288.4828	0.4885	50.4	340.5	...
...	5	54578.986	2.143	0.041	0.373	0.098	278.8586	0.4990	51.7	349.9	...
...	6	54578.993	2.136	0.041	0.363	0.068	274.6806	0.4972	52.0	354.1	...
...	7	54579.001	2.147	0.038	0.372	0.087	270.5102	0.4913	52.1	358.4	...
174897	1	54669.758	2.142	0.029	0.352	0.044	318.2134	0.1688	69.0	337.7	E1-S1
...	2	54669.766	2.120	0.037	0.356	0.043	315.9476	0.1645	69.8	346.0	...
...	3	54669.773	2.127	0.038	0.362	0.041	314.2683	0.1659	70.2	352.4	...
...	4	54669.779	2.116	0.034	0.350	0.037	312.5599	0.1567	70.3	359.0	...
...	5	54669.786	2.136	0.039	0.369	0.038	310.8380	0.1643	70.2	5.7	...
...	6	54669.792	2.128	0.041	0.369	0.059	309.0538	0.1608	69.9	12.7	...
174897	1	54671.782	2.128	0.030	0.345	0.032	261.5103	0.0885	70.2	7.7	E2-S1
...	2	54671.790	2.110	0.030	0.343	0.040	260.4216	0.0799	69.7	15.8	...
...	3	54671.797	2.134	0.023	0.344	0.030	259.6046	0.0677	69.0	22.1	...
...	4	54671.804	2.117	0.035	0.362	0.052	258.8267	0.0654	68.1	28.9	...

Continued on next page

Table B.1 – continued from previous page

HD	Seq #	Obs Date (MJD)	λ_{eff} (μm)	$\sigma\lambda_{eff}$ (μm)	$\Delta\lambda$ (μm)	$\sigma\Delta\lambda$ (μm)	Baseline (m)	Baseline range (m)	Alt (°)	Az (°)	Telescopes used
...	5	54671.810	2.146	0.035	0.361	0.050	258.2350	0.0527	67.1	33.9	...
...	6	54671.817	2.120	0.035	0.344	0.037	257.7325	0.0426	65.9	38.8	...
182572	1	54669.763	2.116	0.030	0.344	0.034	319.3606	0.1609	64.2	326.2	E1-S1
...	2	54669.769	2.121	0.036	0.358	0.041	317.5358	0.1679	65.2	331.0	...
...	3	54669.776	2.139	0.026	0.354	0.035	315.6863	0.1734	66.0	336.1	...
...	4	54669.782	2.152	0.032	0.373	0.051	316.7895	0.1766	66.7	341.5	...
...	5	54669.789	2.122	0.043	0.368	0.053	311.7687	0.1798	67.3	347.3	...
182572	1	54671.787	2.127	0.031	0.345	0.039	260.1586	0.1251	67.5	350.6	E2-S1
...	2	54671.793	2.146	0.031	0.354	0.055	258.9946	0.1135	67.7	356.3	...
...	3	54671.800	2.124	0.031	0.345	0.038	257.7701	0.1067	67.7	2.8	...
...	4	54671.807	2.110	0.032	0.345	0.037	256.6082	0.0932	67.5	9.3	...
...	5	54671.814	2.117	0.039	0.351	0.043	255.6089	0.0851	67.1	15.3	...
182572	1	54739.637	2.115	0.034	0.343	0.020	300.1108	0.1603	66.2	22.8	E1-S1
...	2	54739.644	2.137	0.028	0.347	0.026	298.2793	0.1509	65.3	28.3	...
...	3	54739.680	2.122	0.036	0.343	0.028	291.0932	0.0783	58.4	51.1	...
...	4	54739.686	2.115	0.039	0.343	0.031	290.3447	0.0625	56.9	54.2	...
...	5	54739.693	2.132	0.035	0.342	0.031	289.7269	0.0448	55.2	57.3	...
...	6	54739.700	2.127	0.046	0.352	0.038	289.2970	0.0254	53.4	60.3	...
...	7	54739.707	2.134	0.034	0.347	0.039	289.1126	0.0071	51.6	62.9	...
204965	1	54741.651	2.135	0.035	0.352	0.057	302.7339	0.2673	68.4	205.2	W1-E1
...	2	54741.664	2.118	0.037	0.345	0.062	304.6982	0.3535	69.9	198.3	...
...	3	54741.676	2.121	0.041	0.334	0.114	309.1019	0.1692	70.8	191.0	...
214734	1	54724.877	2.126	0.041	0.354	0.034	282.5724	0.0154	54.4	155.6	E1-S2
...	2	54724.887	2.121	0.044	0.355	0.038	282.7622	0.0073	53.1	154.0	...
...	3	54724.895	2.119	0.036	0.359	0.046	282.8181	0.0008	52.1	152.8	...
265866	1	54761.868	2.125	0.031	0.348	0.046	295.8044	0.4931	42.4	253.9	E1-S1
...	2	54761.882	2.125	0.041	0.365	0.058	303.1378	0.3273	46.3	255.6	...
...	3	54761.891	2.123	0.036	0.361	0.075	307.3806	0.2970	48.9	256.7	...

Continued on next page

Table B.1 – continued from previous page

HD	Seq #	Obs Date (MJD)	λ_{eff} (μm)	$\sigma\lambda_{eff}$ (μm)	$\Delta\lambda$ (μm)	$\sigma\Delta\lambda$ (μm)	Baseline (m)	Baseline range (m)	Alt (°)	Az (°)	Telescopes used
...	4	54761.907	2.119	0.046	0.378	0.080	313.9338	0.2958	53.6	258.7	...
265866	1	54762.969	2.132	0.041	0.366	0.056	298.7876	0.3275	72.7	267.3	W1-E1
...	2	54762.988	2.127	0.037	0.363	0.046	306.5111	0.2136	78.2	270.7	...